ST. XAVIER'S COLLEGE (AUTONOMOUS), KOLKATA

DISTINGUISHING PSEUDOPROGRESSION FROM TRUE PROGRESSION IN GLIOBLASTOMA

Multiparametric MRI-Based Radiomics and Machine Learning Approach

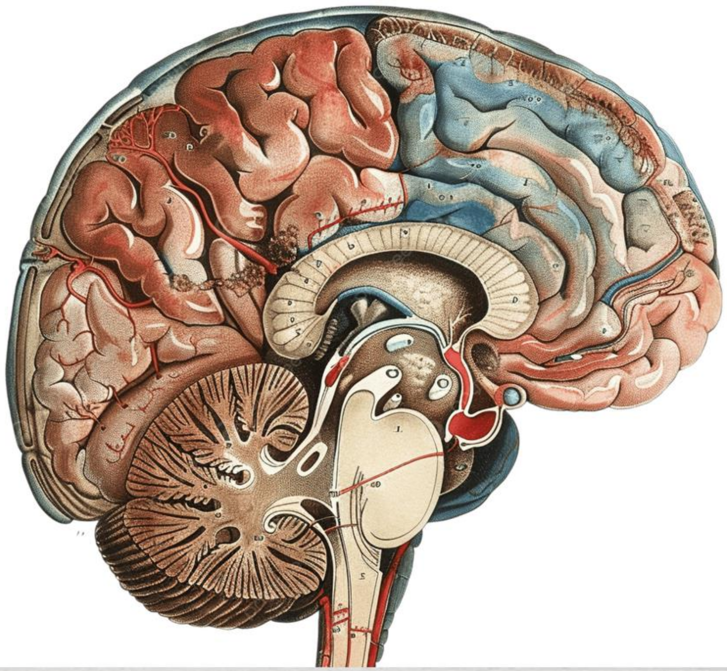

SUPERVISOR

DR. SOURAV BHADURI

Assistant Professor, TCG Crest

INTERNAL MENTOR

DR. ROMIT BEED

Associate Professor, St.Xavier's College

DECLARATION

I affirm that I have identified all my sources and that no part of this dissertation paper contains unacknowledged materials.

DETAILS

SUCHIBRATA PATRA

CIN **24-500-5-08-0403**

Reg **A01-1112-0867-21**

Academic Year **2026**

GETTING TO KNOW

GLIOBLASTOMA

Most malignant primary brain tumour in adults. (*WHO Grade IV*, IDH-wildtype).

45.2%
Of all primary malignant CNS tumours.

14-16 months
Median Survival post-diagnosis

5.5%
5-year survival rate.

~90%
of IDH-wildtype cases arise de novo in older patients

MULTIMODAL CHARACTERIZATION OF GBM

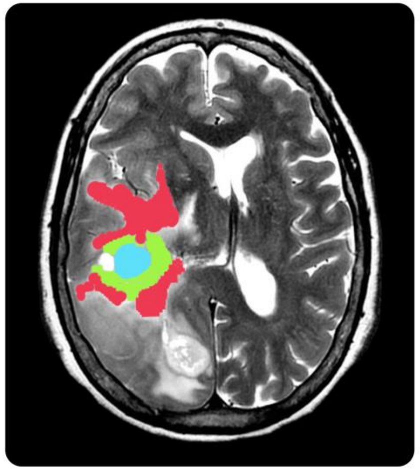

Radiological Image

- Edema Region
- Enhancing Tumor
- Necrotic Core

Description
(A) T2 Weighted MRI Scan With Sub region Markings
(B) Histopathological image of Glioblastoma (Hematoxylin and Eosin stained)

HISTOPATHOLOGICAL IMAGE (H&E STAIN)

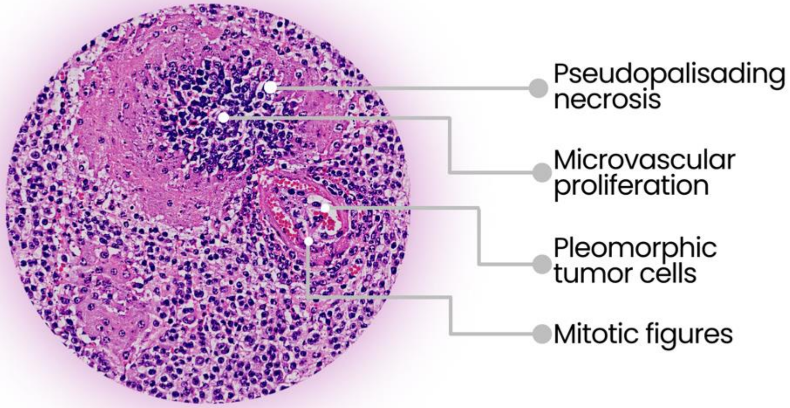

Image Credit - Suchibrata Patra | **Source**: Neuro-Oncology Advanced (Oxford, under review)

When Imaging isn't
ENOUGH

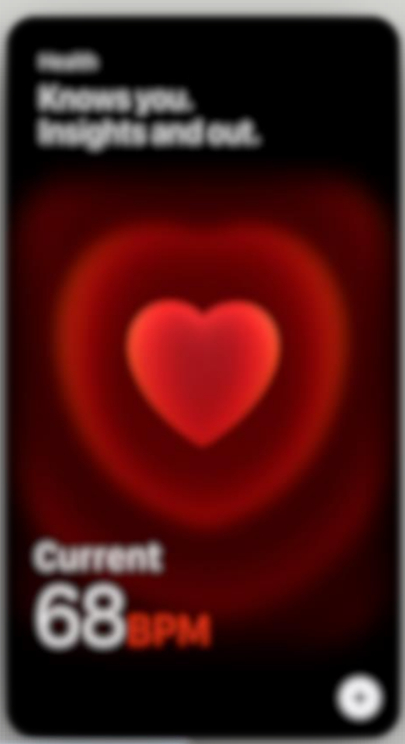

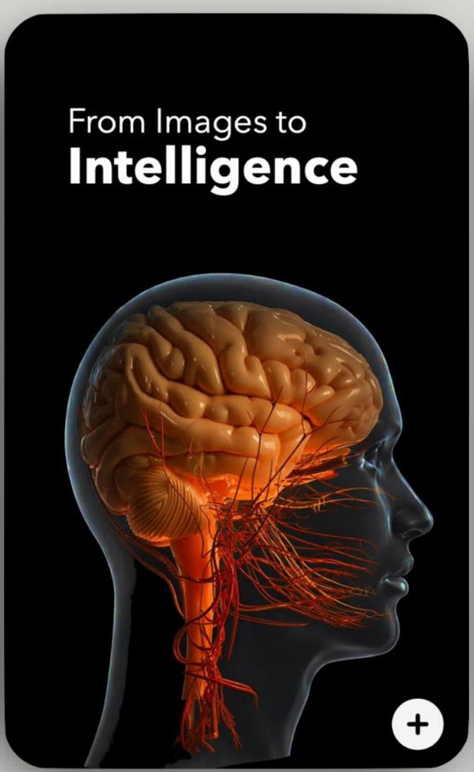

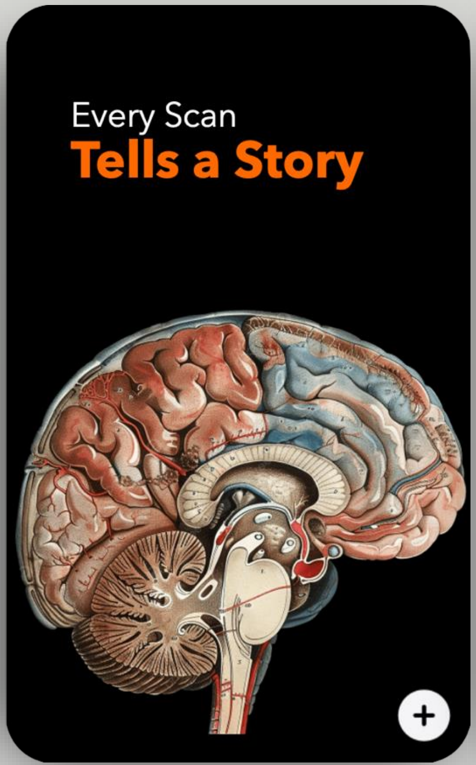

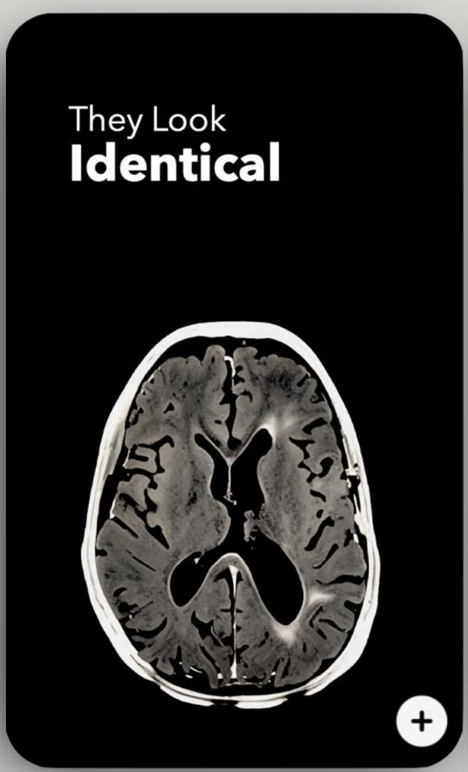

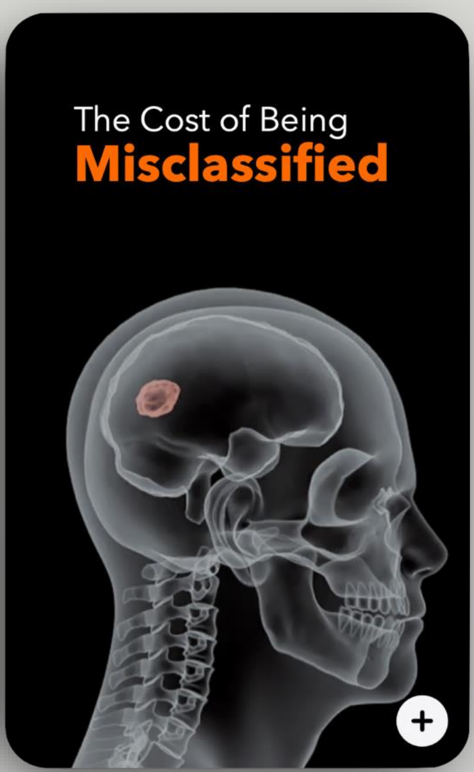

When Imaging isn't **ENOUGH**

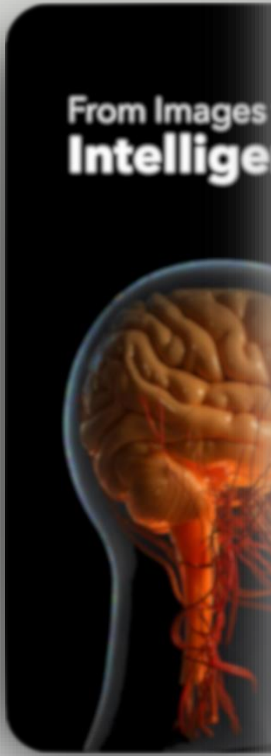

Foundations

A medical scan shows structure, not always clear meaning.

Medical images, specially Magnetic Resonance Imaging give us a detailed view of what's inside the body. We can see shapes, boundaries, and visible biological changes. But not every important detail is clearly obvious. Some differences are very subtle and obvious to overlook, especially in the early stages. So even though the information is there, understanding it completely is not always convenient !

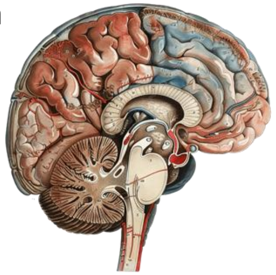

When Imaging isn't
ENOUGH

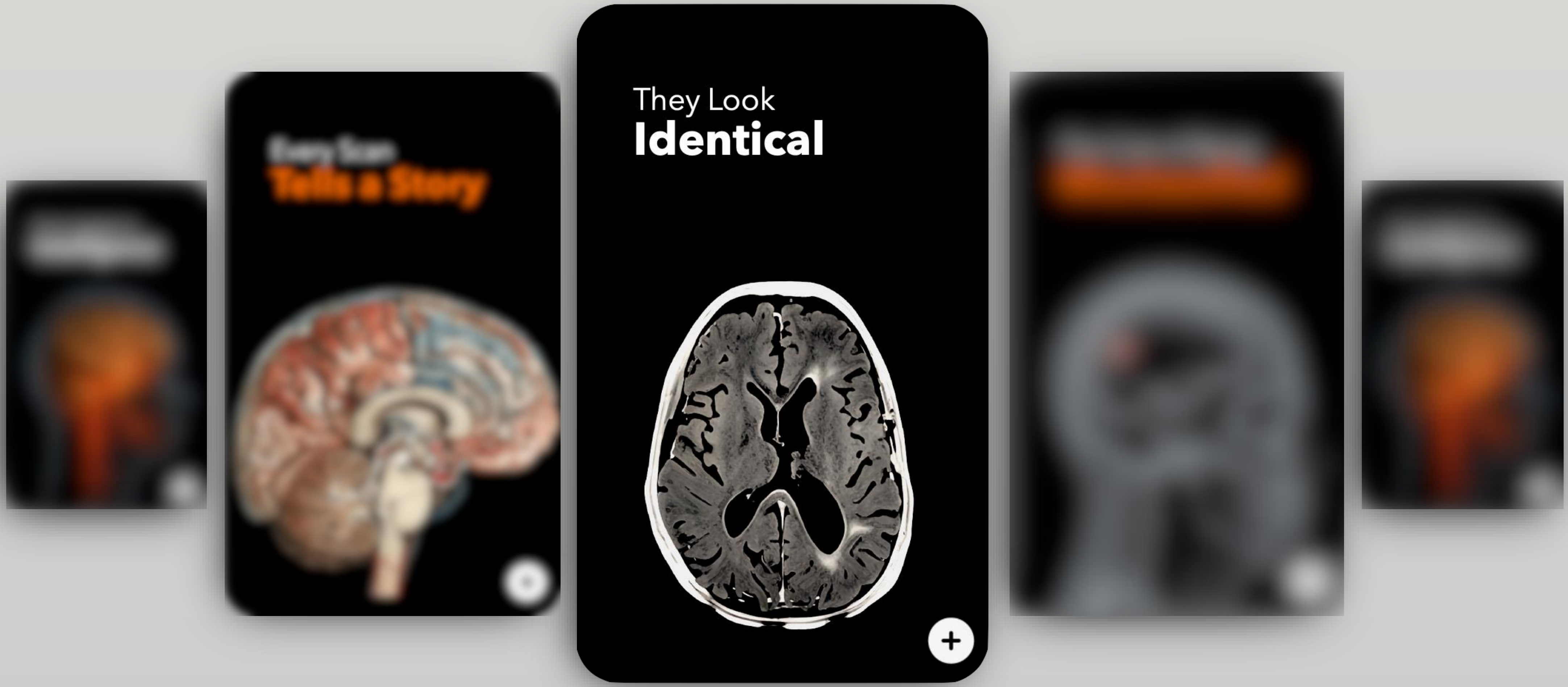

When Imaging isn’t
ENOUGH

Foundations

TP and PSP Often Indistinguishable on Conventional MRI

Both show contrast enhancement and lesion growth due to blood–brain barrier disruption, making them difficult to distinguish.

DICOM Credit : University of Toronto (University Health Network, UHN)

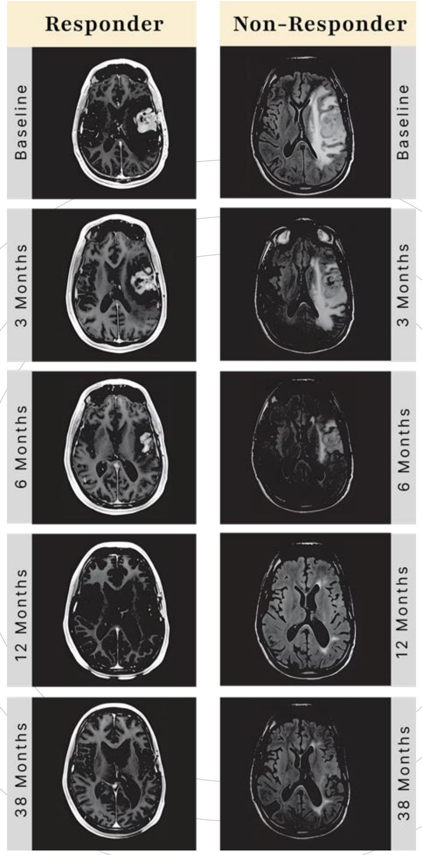

When Imaging isn’t **ENOUGH**

When Imaging isn't
ENOUGH

Foundations

Clinical Consequences of Misclassification

Clinically, this is important. In glioblastoma, different tumour regions can show similar post-treatment changes, making TP and PsP look alike. This can lead to misclassification, resulting in either unnecessary treatment changes or delayed intervention

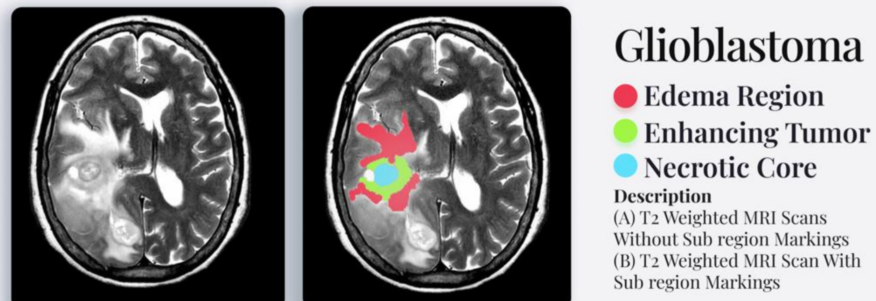

Image Credit : University of Pennsylvania Multi modal Brain Tumor Segmentation Challenge 2020

When Imaging isn’t **ENOUGH**

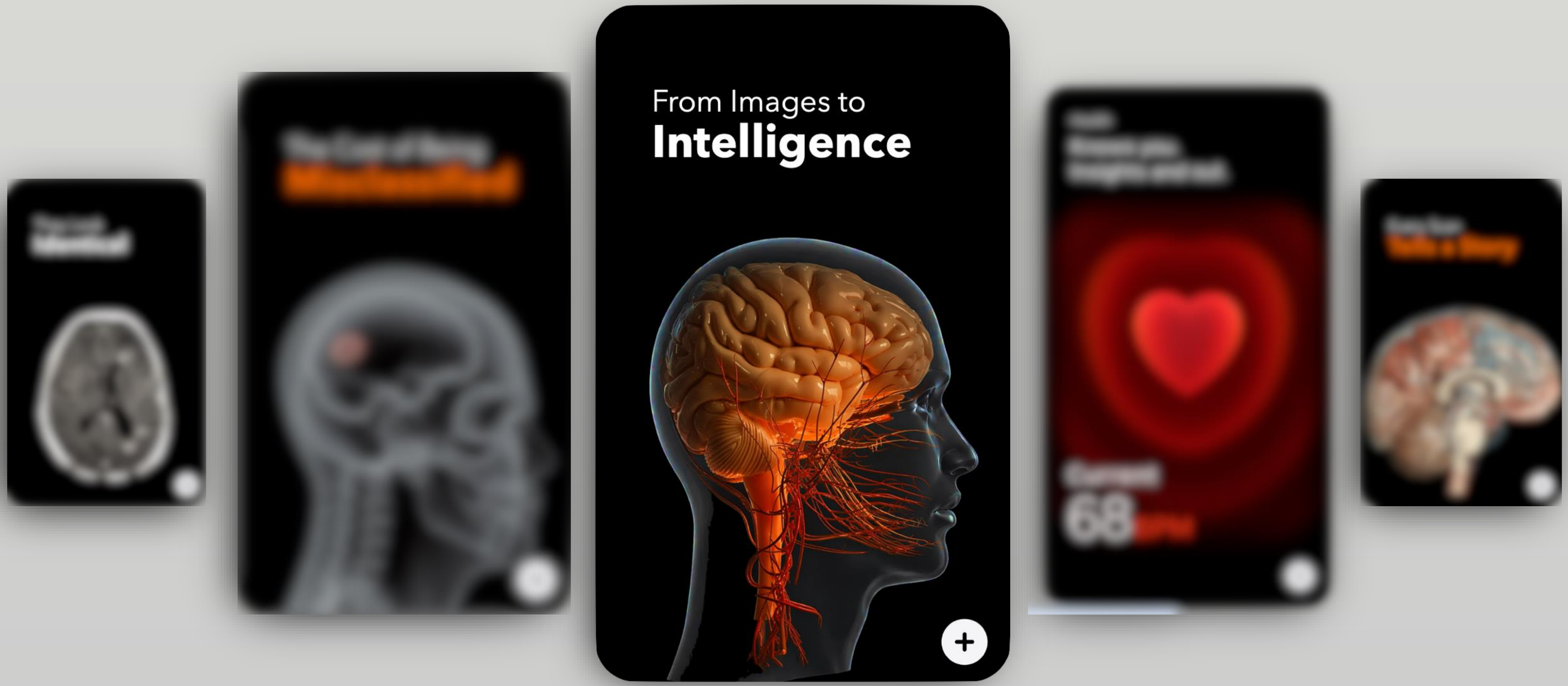

When Imaging isn’t
ENOUGH

Foundations

A medical scan shows structure, not always clear meaning !

Conventionally used software from vendors like GE, Siemens, Philips, along with **conventional models**, remain limited in reliably distinguishing TP from PsP due to imaging regions overlap. Most approaches report performance ≤75% in accuracy. In this work, we adopt a fundamentally novel approach, achieving improved performance with an AUC of 0.89 and an F1-score of 0.90 [Different Gradient Coils too]

QUANTITATIVE PERFUSION IMAGING

Dynamic Contrast Enhanced

DCE MRI

Quantitative assessment of tumour perfusion and microvascular permeability using DCE-MRI

Image courtesy of the National Cancer Institute, via Unsplash*

DCE -MRI PARAMETERS

Key pharmacokinetic parameters that quantifies tissue perfusion and microenvironment

τ_i

Intracellular Water Lifetime

Average time water molecules spend inside cells.

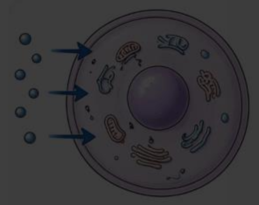

Shorter τ implies higher cell membrane

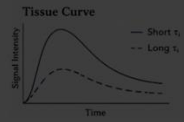

V_p

Plasma Volume Fraction

Fraction of tissue volume occupied by plasma (intravascular space).A

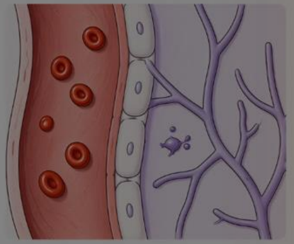

Reflects vascular Volume or Density

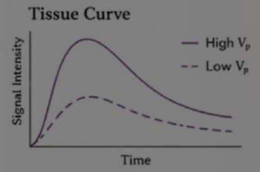

K^{trans}

Volume Transfer Constant

Rate at which contrast moves from plasma to the Extravascular Extracellular Space (EES)

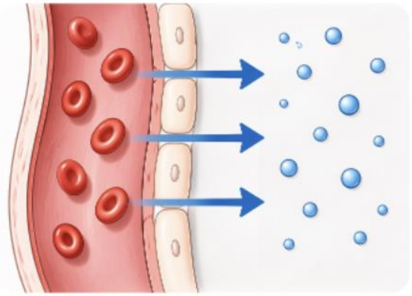

Reflects Capillary Permeability & Surface Area

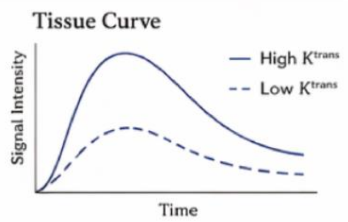

V_e

EES Volume Fraction

Fraction of tissue volume occupied by the Extravascular and Extracellular Space

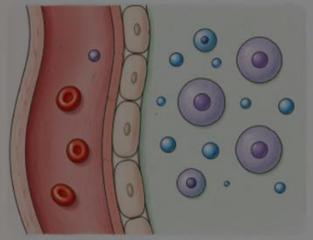

Increased in edema/necrosis & lower in dense tumour

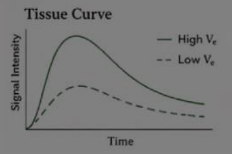

F_p

Plasma Flow Rate

Rate of plasma flowing through the capillary bed per unit tissue volume.

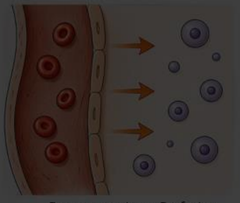

Represents tissue Perfusion

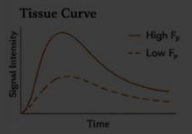

Image Credit: Adapted from Jain & Essig, Dynamic Contrast-Enhanced MRI (Thieme Medical Publishers)

DCE -MRI PARAMETERS

Key pharmacokinetic parameters that quantifies tissue perfusion and microenvironment

V_p

Plasma Volume Fraction

Fraction of tissue volume occupied by plasma (intravascular space).A

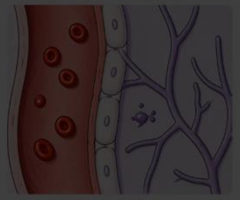

Reflects vascular Volume or Density

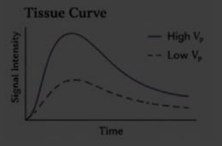

K^{trans}

Volume Transfer Constant

Rate at which contrast moves from plasma to the Extravascular Extracellular Space (EES)

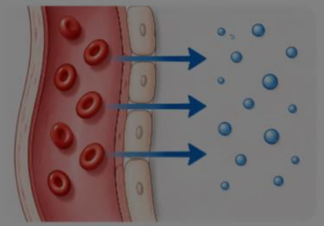

Reflects Capillary Permeability & Surface Area

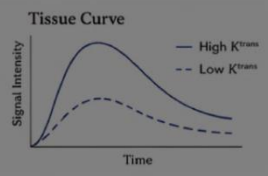

V_e

EES Volume Fraction

Fraction of tissue volume occupied by the Extravascular and Extracellular Space

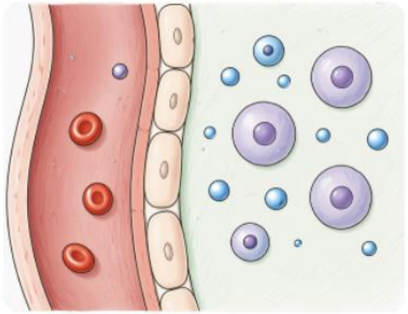

Increased in edema/necrosis & lower in dense tumour

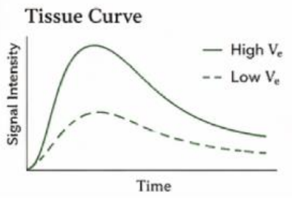

F_p

Plasma Flow Rate

Rate of plasma flowing through the capillary bed per unit tissue volume.

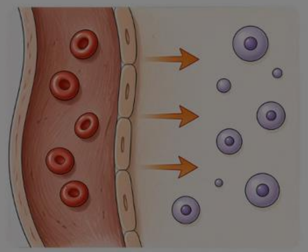

Represents tissue Perfusion

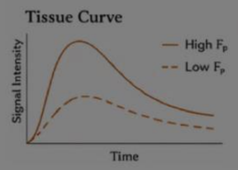

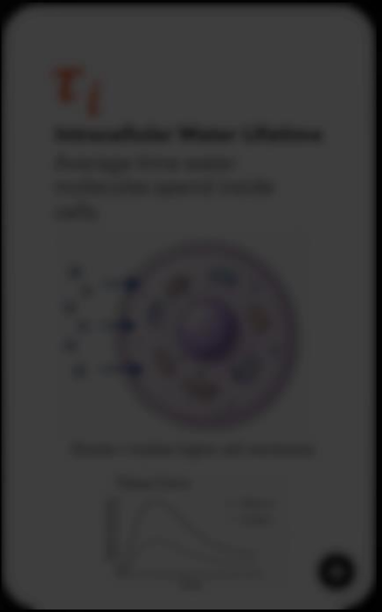

Image Credit: Adapted from Jain & Essig, Dynamic Contrast-Enhanced MRI (Thieme Medical Publishers)

DCE MRI PARAMETERS

Key pharmacokinetic parameters that quantifies tissue perfusion and microenvironment

K^{trans}

Volume Transfer Constant

Rate at which contrast moves from plasma to the Extravascular Extracellular Space (EES)

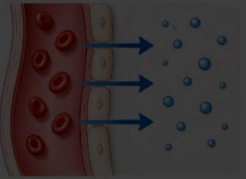

Reflects Capillary Permeability & Surface Area

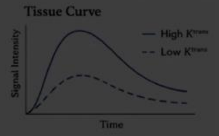

V_e

EES Volume Fraction

Fraction of tissue volume occupied by the Extravascular and Extracellular Space

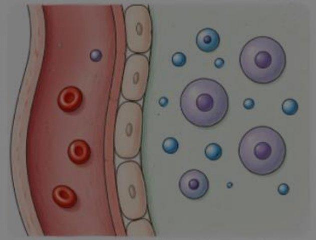

Increased in edema/necrosis & lower in dense tumour

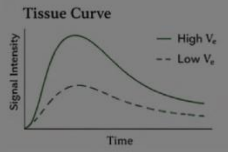

F_p

Plasma Flow Rate

Rate of plasma flowing through the capillary bed per unit tissue volume.

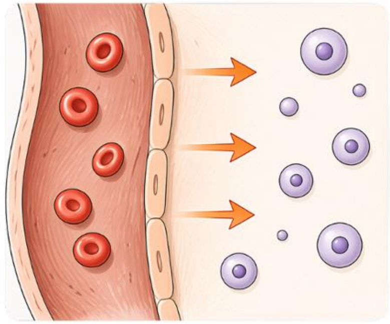

Represents tissue Perfusion

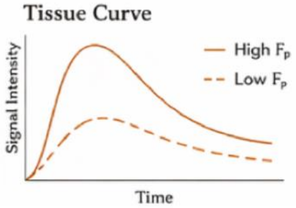

τ_i

Intracellular Water Lifetime

Average time water molecules spend inside cells.

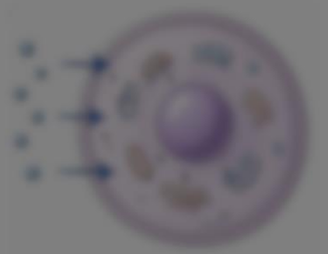

V_p

Plasma Volume Fraction

Fraction of tissue volume occupied by plasma (intravascular space).A

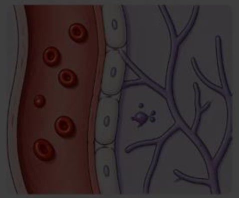

Reflects vascular Volume or Density

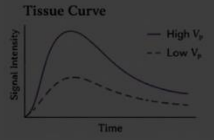

Image Credit: Adapted from Jain & Essig, Dynamic Contrast-Enhanced MRI (Thieme Medical Publishers)

DCE MRI PARAMETERS

Key pharmacokinetic parameters that quantifies tissue perfusion and microenvironment

V_e

EES Volume Fraction

Fraction of tissue volume occupied by the Extravascular and Extracellular Space

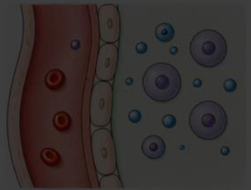

Increased in edema/necrosis & lower in dense tumour

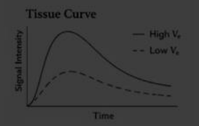

F_p

Plasma Flow Rate

Rate of plasma flowing through the capillary bed per unit tissue volume.

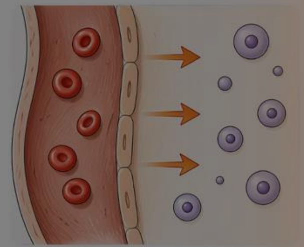

Represents tissue Perfusion

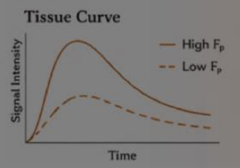

τ_i

Intracellular Water Lifetime

Average time water molecules spend inside cells.

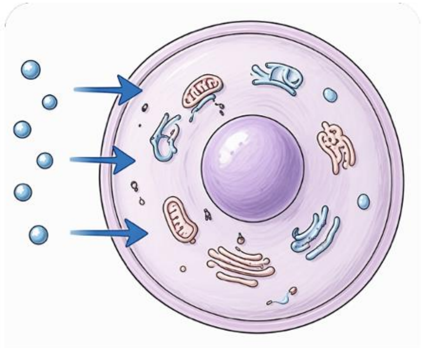

Shorter τ implies higher cell membrane

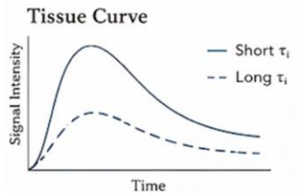

V_p

Plasma Volume Fraction

Fraction of tissue volume occupied by plasma (intravascular space).A

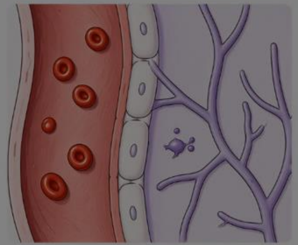

Reflects vascular Volume or Density

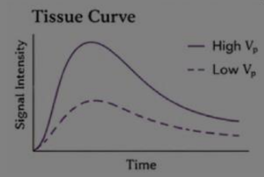

K^{trans}

Volume Transfer Constant

Rate at which contrast moves from plasma to the Extravascular Extracellular Space (EES)

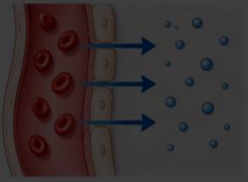

Reflects Capillary Permeability & Surface Area

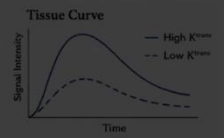

Image Credit: Adapted from Jain & Essig, Dynamic Contrast-Enhanced MRI (Thieme Medical Publishers)

QUANTITATIVE PERFUSION IMAGING

DCE MRI PARAMETERS

Key pharmacokinetic parameters that quantifies tissue perfusion and microenvironment

F_p

Plasma Flow Rate
Rate of plasma flowing through the capillary bed per unit tissue volume.

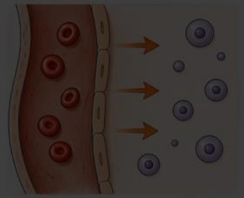

Represents tissue Perfusion

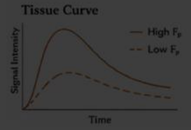

τ_i

Intracellular Water Lifetime
Average time water molecules spend inside cells.

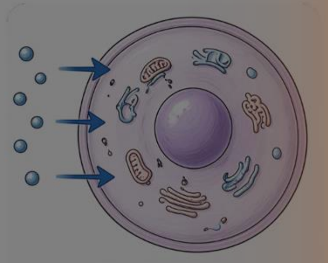

Shorter τ implies higher cell membrane

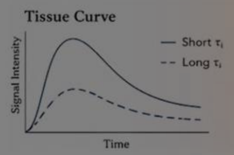

V_p

Plasma Volume Fraction
Fraction of tissue volume occupied by plasma (intravascular space).A

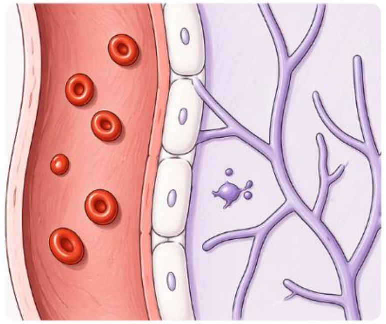

Reflects vascular Volume or Density

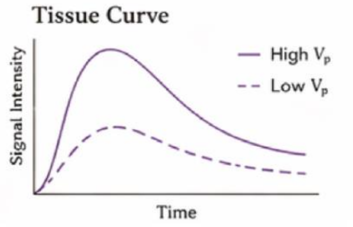

K^{trans}

Volume Transfer Constant
Rate at which contrast moves from plasma to the Extravascular Extracellular Space (EES)

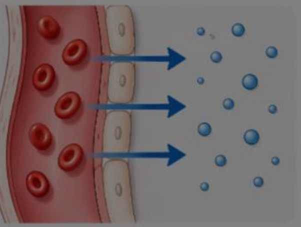

Reflects Capillary Permeability & Surface Area

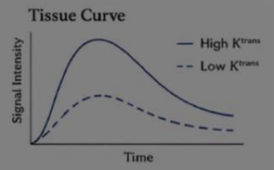

V_e

EES Volume Fraction
Fraction of tissue volume occupied by the Extravascular and Extracellular Space

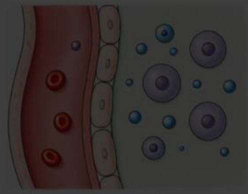

Increased in edema/necrosis & lower in dense tumour

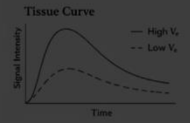

Image Credit: Adapted from Jain & Essig, Dynamic Contrast-Enhanced MRI (Thieme Medical Publishers)

QUANTITATIVE PERFUSION IMAGING

DCE MRI PARAMETERS

Key pharmacokinetic parameters that quantifies tissue perfusion and microenvironment

F_p

Plasma Flow Rate

Rate of plasma flowing through the capillary bed per unit tissue volume.

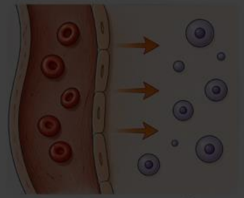

Represents tissue Perfusion

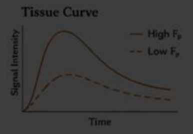

τ_i

Intracellular Water Lifetime

Average time water molecules spend inside cells.

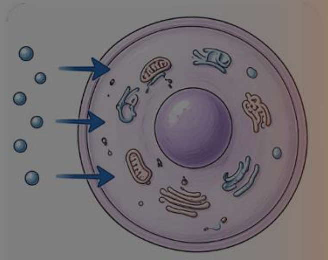

Shorter τ implies higher cell membrane

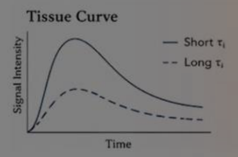

V_p

Plasma Volume Fraction

Fraction of tissue volume occupied by plasma (intravascular space).A

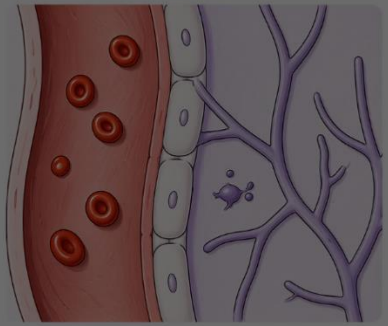

Reflects vascular Volume or Density

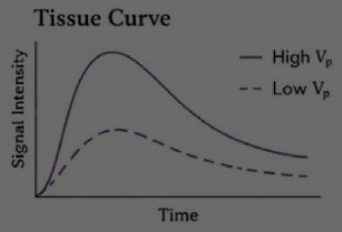

K^{trans}

Volume Transfer Constant

Rate at which contrast moves from plasma to the Extravascular Extracellular Space (EES)

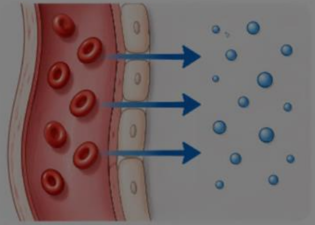

Reflects Capillary Permeability & Surface Area

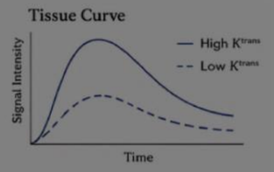

V_e

EES Volume Fraction

Fraction of tissue volume occupied by the Extravascular and Extracellular Space

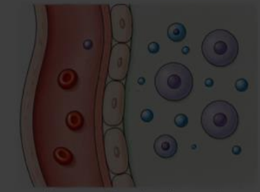

Increased in edema/necrosis & lower in dense tumour

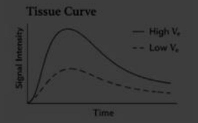

DCE MRI PARAMETERS

Key pharmacokinetic p...
quantifies tissue perfu...
microenvironment

F_p

Plasma Flow Rate
Rate of plasma flowing through the capillary bed per unit tissue volume.

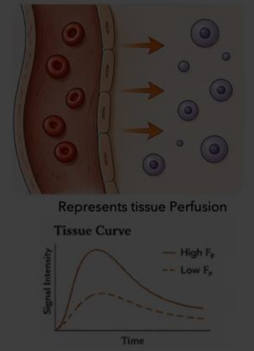

Foundations

TP vs PSP for Several Parametric Maps

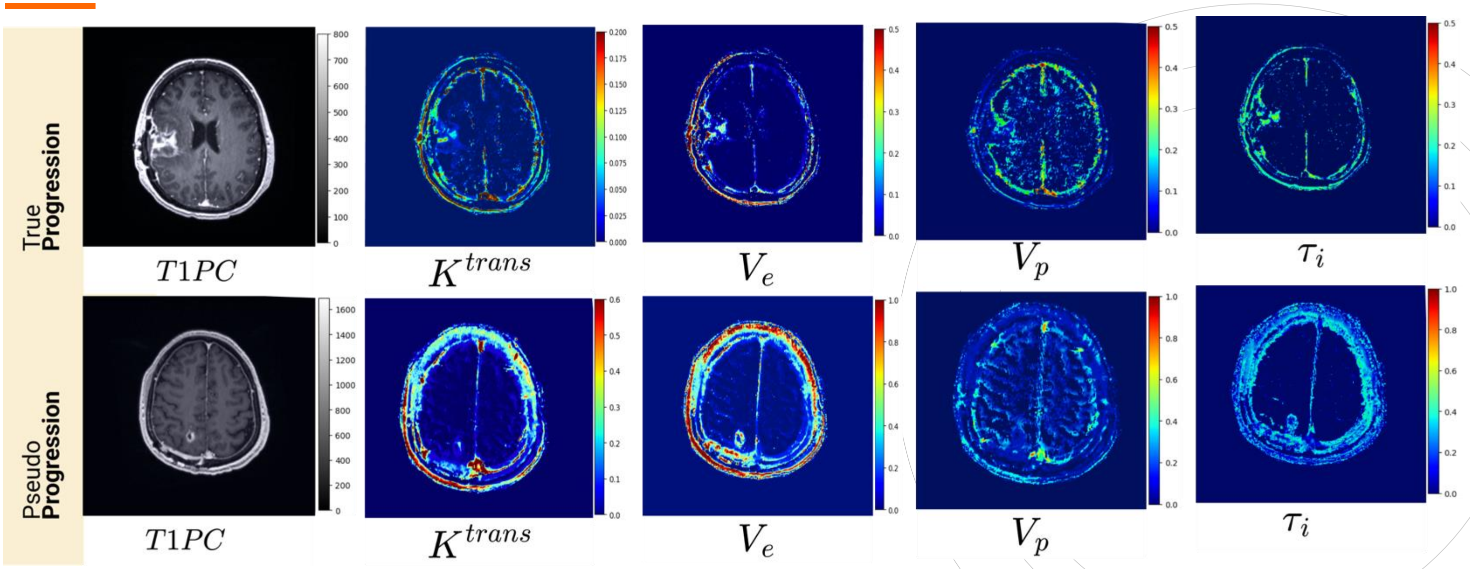

DICOM Credit : University of Pennsylvania

V_e

EES Volume Fraction
Fraction of tissue volume occupied by the Extravascular and Extracellular Space

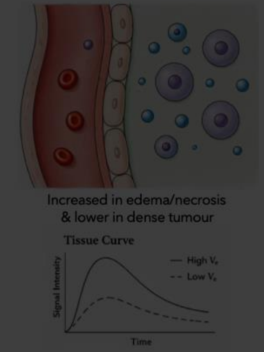

Graphical ABSTRACT

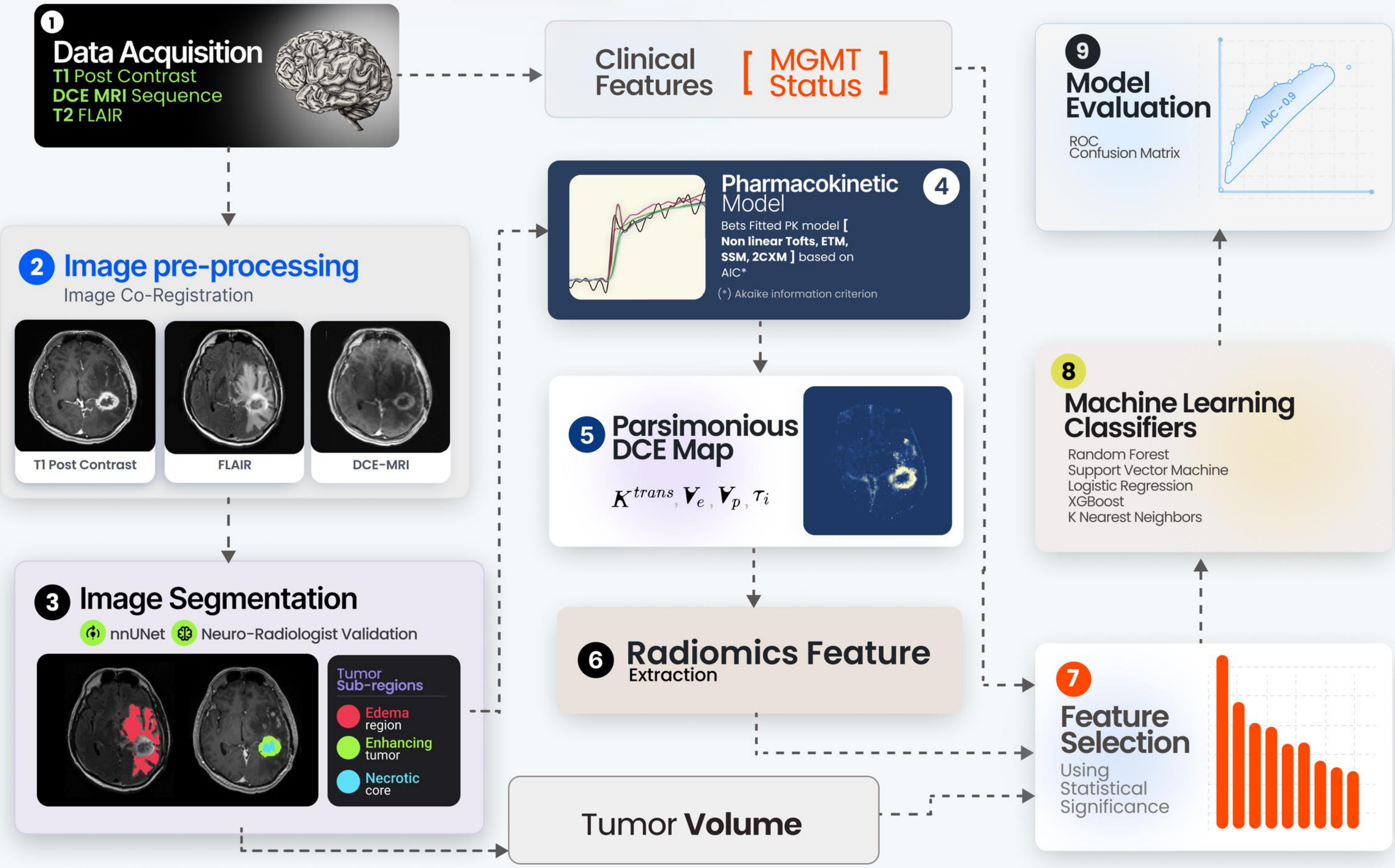

Image Credit - Suchibrata Patra | Source: Neuro-Oncology Advanced (Oxford, under review)

Clinical Data ACQUISITION

All the patients were receipt of standard of care (SOC) therapy, including surgery followed by concurrent chemoradiotherapy (CCRT)

Siemens Healthineers, Erlangen(Germany), a classic 3T MAGNETOM Trio whole-body MR scanner with a 12 channel phased array head coil.

MultiHance, Bracco Imaging, Milano, Italy, a widely used **GCA (Gadolinium Based Contrast Agents)** stain is used, at a dose of 0.07 mmol/kg.
Delivered using a **power injector (Medrad, Indianola, PA, USA).**

A total of **30** sequential measurements were acquired for each slice to assess contrast **wash in - washout** kinetics. [Temporal resolution : **7** seconds per frame]

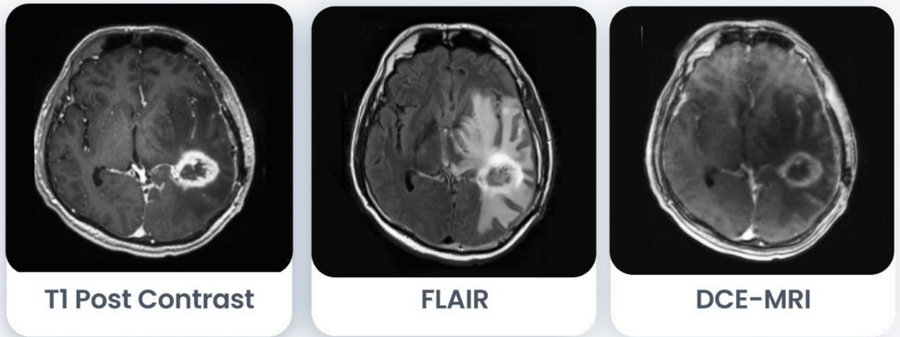

Figure A : Representative multiparametric MRI sequences (T1+C, FLAIR, DCE)

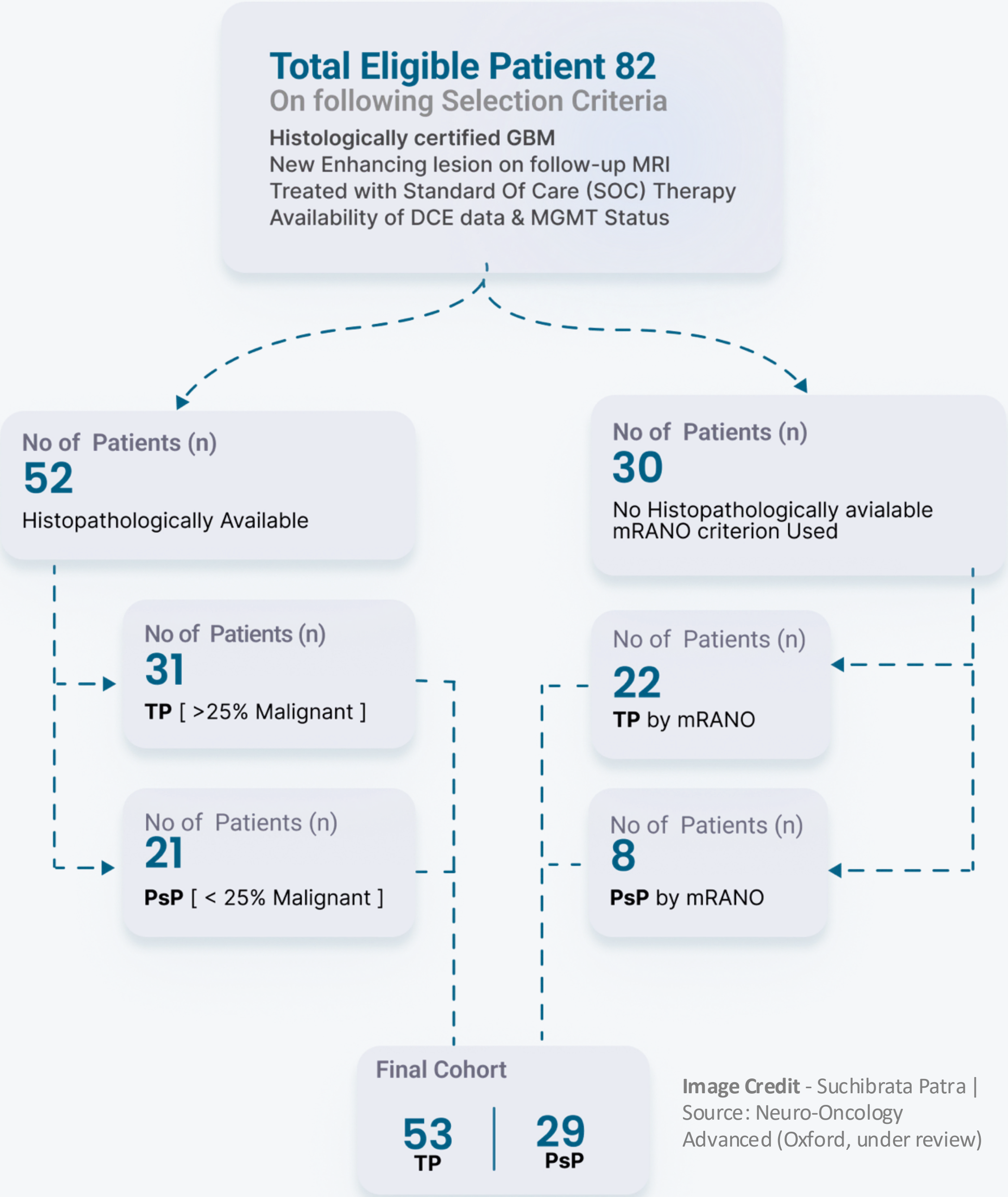

Image Credit - Suchibrata Patra | Source: Neuro-Oncology Advanced (Oxford, under review)

Parameter Maps EXTRAXTION

We began by generating **DCE-MRI parametric maps**, extracting key physiological parameters including Ktrans, VE, Vp, Kep, tau

In-house developed MATLAB toolbox was used, incorporating multiple pharmacokinetic models such as Tofts, ETM, SSM, 2CXM, and 3S2X.

A subject-specific vascular input function (VIF) was then defined by placing an ROI over the superior sagittal sinus (SSS).

Following map generation, **post-contrast T1 and T2-FLAIR images** were co-registered and resliced to align with the DCE-MRI space.
[Rigid Body Affine Transformation was used]

Tumours were segmented using nnU-Net [**Gold standard** as a strong baseline, trained on BraTS dataset 2018-21] on co-registered PC-T1 and FLAIR images (Dice: 88.95%, BraTS), and volume was computed as voxel count × voxel size.

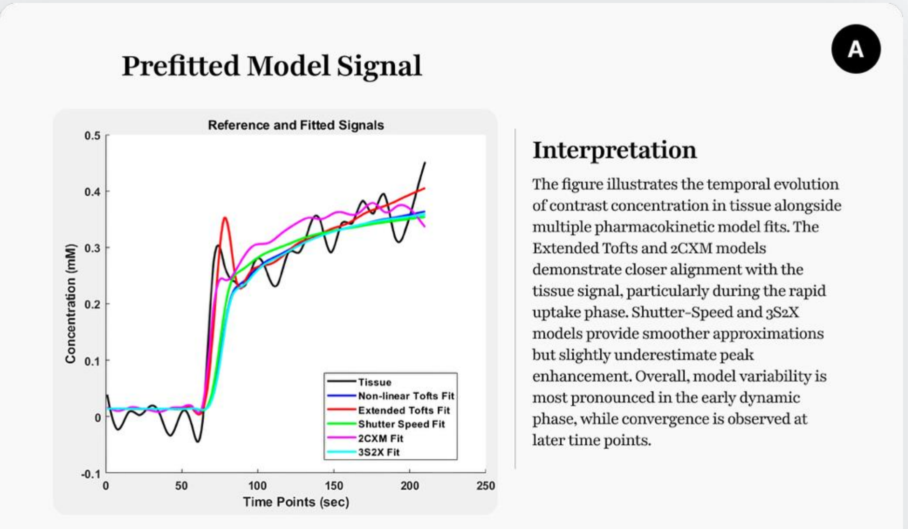

Image Credit : Suchibrata Patra | Source: Neuro-Oncology Advanced (Oxford, under review)

Figure
A. Graph showing the Pre - fitted model signals vs the actual signal
B. MATLAB Toolbox (Developed Inhouse for feature Extraction)

Robust Feature
SELECTION

First Stage Selection

We performed feature selection using a two-stage reduction pipeline, motivated by the high dimensionality of radiomic features (n = 1073) relative to sample size, where overfitting becomes inevitable without proper reduction.

In the first stage, the Non-Parametric Mann–Whitney U test was applied to evaluate the discriminatory power of each feature between TP and PsP. Features with **$p < 0.05$** were retained, reducing the feature space from 1073 to 86.

In the second stage, **Elastic Net regularization** (With L1 (sparsity) and L2 (grouping) penalties) was employed to further refine the feature set.

The hyperparameters (α, ρ) were optimized using grid search with five-fold stratified cross-validation, ensuring class balance across folds and robust generalization.

Second Stage Selection

To address class imbalance (TP > PsP), **ADASYN** was applied to the training set, which adaptively generates synthetic minority samples near decision boundaries, improving learning in difficult areas.
Kept the test set untouched to prevent data leakage.

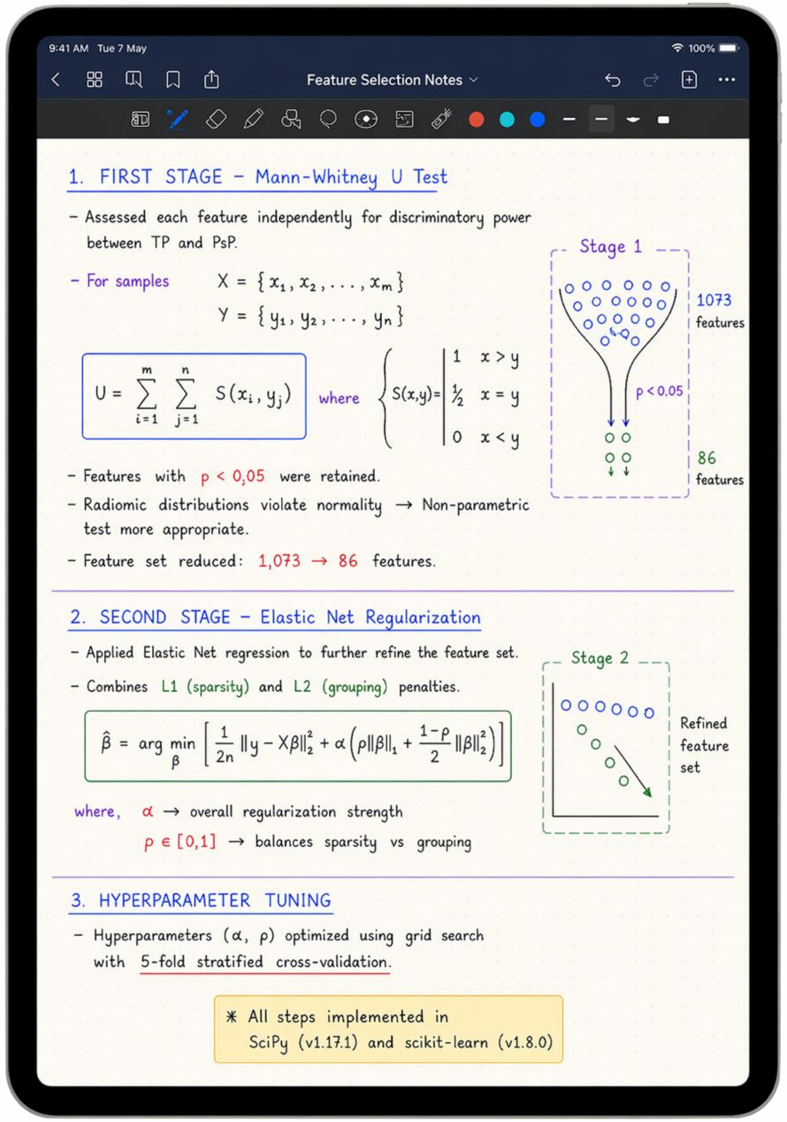

Machine Learning RESULTS

Method	TA	VA	VAUC	TEAUC	TE	Precision	Sensitivity	Specificity	F1
KNN	0.93 ± 0.12	0.69 ± 0.04	0.73 ± 0.05	0.63 ± 0.07	0.62 ± 0.10	0.67 ± 0.13	0.62 ± 0.16	0.60 ± 0.17	0.64 ± 0.13
LR	0.72 ± 0.05	0.67 ± 0.05	0.72 ± 0.04	0.62 ± 0.13	0.58 ± 0.08	0.64 ± 0.10	0.68 ± 0.17	0.43 ± 0.28	0.64 ± 0.08
RF	0.96 ± 0.05	0.63 ± 0.07	0.70 ± 0.08	0.68 ± 0.13	0.64 ± 0.14	0.63 ± 0.13	0.82 ± 0.19	0.38 ± 0.12	0.70 ± 0.13
SVM	0.72 ± 0.15	0.67 ± 0.07	0.70 ± 0.06	0.62 ± 0.08	0.66 ± 0.17	0.69 ± 0.16	0.74 ± 0.24	0.45 ± 0.32	0.67 ± 0.12
XGB	0.88 ± 0.15	0.62 ± 0.07	0.71 ± 0.07	0.61 ± 0.15	0.58 ± 0.13	0.59 ± 0.12	0.71 ± 0.17	0.35 ± 0.16	0.64 ± 0.13

Extended Tofts Model [ETM] + MGMT

No model achieved meaningful discrimination (TEAUC ≤ 0.68), with high training but poor validation performance indicating strong overfitting especially in **RF and XGB** and unstable specificity making the models clinically unreliable.

Method	TA	VA	VAUC	TEAUC	TE	Precision	Sensitivity	Specificity	F1
KNN	1.00 ± 0.00	0.71 ± 0.03	0.81 ± 0.03	0.75 ± 0.06	0.67 ± 0.06	0.74 ± 0.11	0.76 ± 0.16	0.56 ± 0.23	0.73 ± 0.07
LR	0.75 ± 0.04	0.69 ± 0.04	0.76 ± 0.04	0.75 ± 0.07	0.67 ± 0.05	0.77 ± 0.13	0.71 ± 0.11	0.62 ± 0.25	0.72 ± 0.04
RF	1.00 ± 0.00	0.75 ± 0.04	0.83 ± 0.03	0.72 ± 0.05	0.67 ± 0.05	0.73 ± 0.11	0.79 ± 0.17	0.51 ± 0.23	0.74 ± 0.06
SVM	0.97 ± 0.03	0.78 ± 0.06	0.81 ± 0.06	0.72 ± 0.13	0.69 ± 0.09	0.78 ± 0.11	0.72 ± 0.17	0.66 ± 0.20	0.74 ± 0.08
XGB	0.99 ± 0.04	0.73 ± 0.04	0.82 ± 0.04	0.72 ± 0.09	0.67 ± 0.07	0.74 ± 0.08	0.73 ± 0.11	0.58 ± 0.15	0.73 ± 0.07

T1 Post Contrast Model [ETM] + MGMT

SVM provides the best overall balance. **RF** attains the highest VAUC (0.83) but suffers from low specificity, and **LR** remains competitive indicating partial linear separability in the features.

Model	TA	VA	TEAUC	TE	Precision	Sensitivity	Specificity	F1
RF	1.00 ± 0.00	0.75 ± 0.03	0.84 ± 0.09	0.79 ± 0.09	0.82 ± 0.12	0.91 ± 0.13	0.57 ± 0.31	0.85 ± 0.07
KNN	1.00 ± 0.00	0.72 ± 0.04	0.80 ± 0.09	0.66 ± 0.10	0.74 ± 0.11	0.75 ± 0.14	0.48 ± 0.23	0.74 ± 0.10
LR	0.74 ± 0.04	0.69 ± 0.05	0.74 ± 0.06	0.72 ± 0.05	0.80 ± 0.08	0.78 ± 0.11	0.62 ± 0.14	0.78 ± 0.06
SVM	0.88 ± 0.09	0.77 ± 0.04	0.76 ± 0.12	0.80 ± 0.10	0.75 ± 0.17	0.62 ± 0.17	0.77 ± 0.12	0.73 ± 0.06
XGB	0.99 ± 0.02	0.71 ± 0.03	0.81 ± 0.09	0.74 ± 0.10	0.83 ± 0.12	0.81 ± 0.17	0.63 ± 0.26	0.80 ± 0.10

Parsimonious DCE Parameters

RF delivers the highest TEAUC (0.84 ± 0.09) and sensitivity (0.91 ± 0.13), showing improved feature quality, but its specificity is low and unstable, while SVM offers the best specificity (0.77 ± 0.12) with a slightly lower yet acceptable TEAUC.

Models	TA	VA	VAUC	TEAUC	TE	Precision	Sensitivity	Specificity	F1
RF	1.0 ± 0	0.74 ± 0.03	0.82 ± 0.03	0.89 ± 0.07	0.86 ± 0.1	0.88 ± 0.1	0.93 ± 0.09	0.76 ± 0.19	0.9 ± 0.07
KNN	1.00 ± 0.00	0.70 ± 0.05	0.78 ± 0.04	0.73 ± 0.11	0.67 ± 0.11	0.74 ± 0.09	0.77 ± 0.17	0.46 ± 0.17	0.75 ± 0.1
LR	0.73 ± 0.04	0.67 ± 0.05	0.72 ± 0.05	0.72 ± 0.05	0.67 ± 0.08	0.76 ± 0.1	0.76 ± 0.13	0.51 ± 0.3	0.76 ± 0.06
SVM	0.89 ± 0.12	0.73 ± 0.07	0.75 ± 0.05	0.71 ± 0.14	0.64 ± 0.12	0.73 ± 0.11	0.73 ± 0.18	0.45 ± 0.22	0.72 ± 0.11
XGB	0.98 ± 0.04	0.69 ± 0.07	0.78 ± 0.04	0.79 ± 0.09	0.72 ± 0.11	0.79 ± 0.12	0.82 ± 0.16	0.56 ± 0.27	0.79 ± 0.08

Parsimonious DCE + MGMT

RF achieves the best overall performance (TEAUC 0.89, sensitivity 0.93, specificity 0.76, F1 0.90) and is the recommended deployment model, with clear gains over the MGMT-free setup highlighting the strong added value of molecular biomarker integration.

Gini Feature IMPORTANCE

Parsimonious Without MGMT
Gini Importance

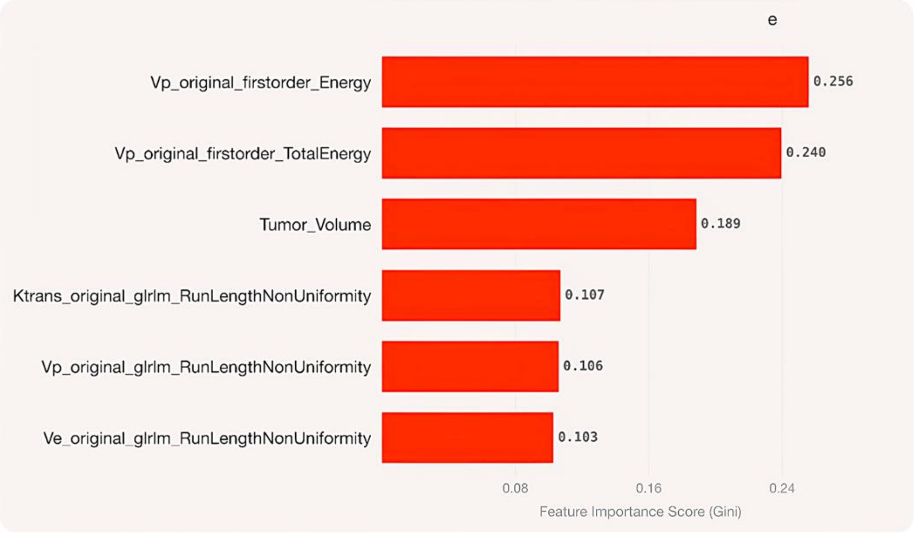

Extended TOFTS with MGMT
Gini Importance

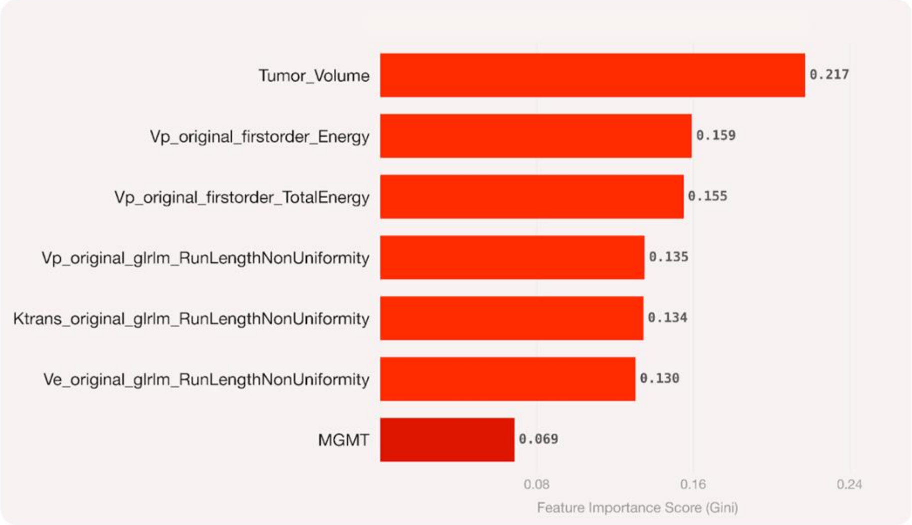

T1 Post Contrast with MGMT
Gini Importance

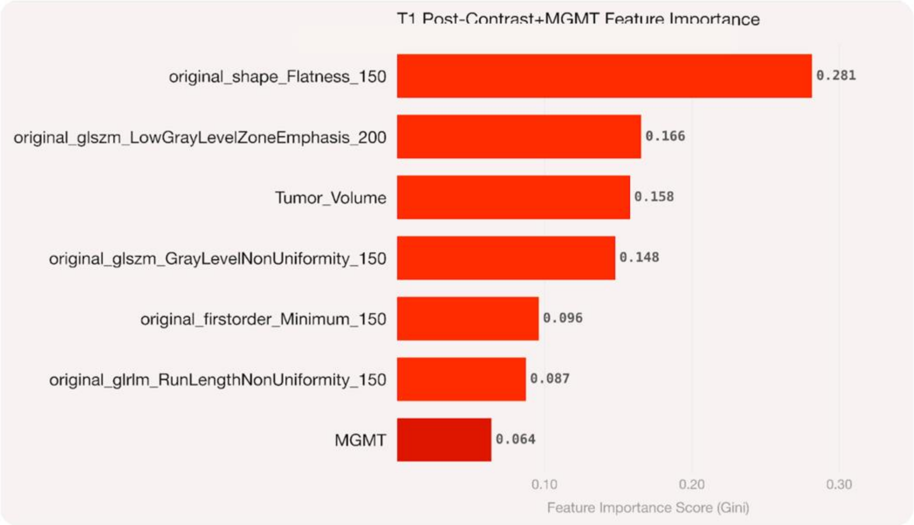

Parsimonious + MGMT
Gini Importance

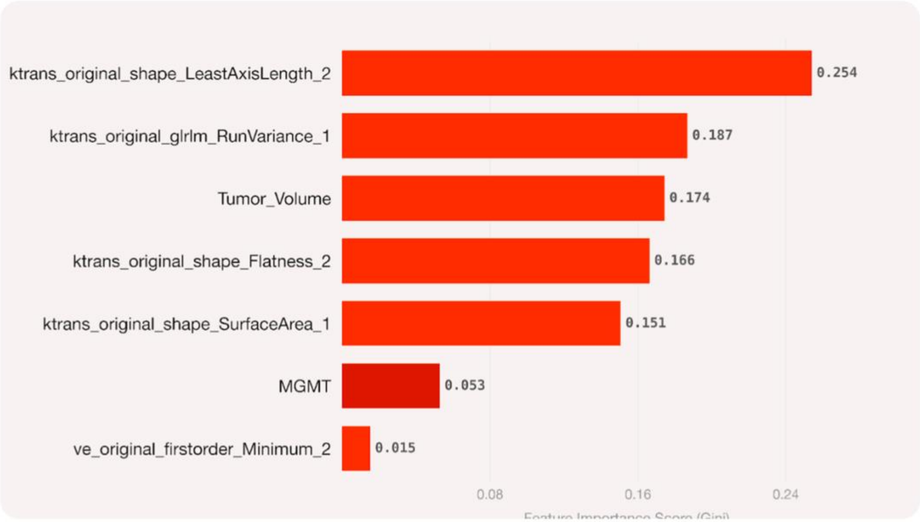

DISCUSSION & CONCLUSION

Discussion & Clinical Significance

Parsimonious DCE + MGMT + RF achieves SOTA performance (TEAUC 0.89, Sens 0.93, Spec 0.76), confirming optimal feature–model synergy

Parsimonious PK modelling + MGMT integration significantly enhance discriminative power over conventional approaches

Random Forest effectively captures complex, non-linear radiomic interactions, outperforming linear and boosting models

Enables high-confidence, non-invasive TP vs PsP differentiation, addressing a critical clinical uncertainty

Study Limitations

Small, yet imbalanced cohort **(n=82)**

Single centre data, that's why scanner/protocol dependency may affect robustness

Mixed ground truth (histology + mRANO) → potential label inconsistency

No external validation has been performed. So, in reality the true generalisation still remains unproven

Additional Constraints
Cross-sectional design - ignores longitudinal disease evolution.
MGMT ambiguity (indeterminate cases) reduces interpretability
.
Limited clinical interpretability, because that requires SHAP.

References

References

1. Kanderi T, Munakomi S, Gupta V. GBM Multiforme. [Updated 2024 May 6]. In: StatPearls [Internet]. Treasure Island (FL): StatPearls Publishing; 2026 Jan-. Available from: https://www.ncbi.nlm.nih.gov/books/NBK558954/
2. Antonelli M, Poliani PL. Adult type diffuse gliomas in the new 2021 WHO Classification. Pathologica. 2022 Dec;114(6):397-409. doi: 10.32074/1591-951X-823. PMID: 36534419; PMCID: PMC9763975.
3. Huang LL, Xia HH, Zhu SL. Ascitic Fluid Analysis in the Differential Diagnosis of Ascites: Focus on Cirrhotic Ascites. J Clin Transl Hepatol. 2014;2(1):58-64. doi:10.14218/JCTH.2013.00010
4. Young JS, Al-Adli N, Sibih YE, Cha S, Berger MS. Pseudoprogression versus true progression in glioblastoma: what neurosurgeons need to know. J Neurosurg. 2023;139(3):748–759. DOI: 10.3171/2022.12.JNS222173 · PMID: 36774577
5. Strauss SB, Meng A, Ebani EJ, Chiang GC. Imaging Glioblastoma Posttreatment: Progression, Pseudoprogression, Pseudoresponse, Radiation Necrosis. Radiol Clin North Am. 2019;57(6):1199-1216. doi:10.1016/j.rcl.2019.07.003
6. Hygino da Cruz LC Jr, Rodriguez I, Domingues RC, Gasparetto EL, Sorensen AG. Pseudoprogression and pseudoresponse: imaging challenges in the assessment of posttreatment glioma. AJNR Am J Neuroradiol. 2011;32(11):1978-1985. doi:10.3174/ajnr.A2397
7. Pooley RA. AAPM/RSNA physics tutorial for residents: fundamental physics of MR imaging. Radiographics. 2005;25(4):1087-1099. doi:10.1148/rg.254055027
8. Grover VP, Tognarelli JM, Crossey MM, Cox IJ, Taylor-Robinson SD, McPhail MJ. Magnetic Resonance Imaging: Principles and Techniques: Lessons for Clinicians. J Clin Exp Hepatol. 2015;5(3):246-255. doi:10.1016/j.jceh.2015.08.001
9. Currie S, Hoggard N, Craven IJ, Hadjivassiliou M, Wilkinson ID. Understanding MRI: basic MR physics for physicians. Postgrad Med J. 2013;89(1050):209-223. doi:10.1136/postgradmedj-2012-131342
10. MRI From Picture to Proton: 2nd ed. AJNR Am J Neuroradiol. 2008;29(6):e50. doi:10.3174/ajnr.A0980
11. Gonçalves FG, Chawla S, Mohan S. Emerging MRI Techniques to Redefine Treatment Response in Patients With Glioblastoma. J Magn Reson Imaging. 2020;52(4):978-997. doi:10.1002/jmri.27105
12. Sourbron SP, Buckley DL. Classic models for dynamic contrast-enhanced MRI. NMR Biomed. 2013;26(8):1004-1027. doi:10.1002/nbm.2940
13. Tofts PS, Brix G, Buckley DL, et al. Estimating kinetic parameters from dynamic contrast-enhanced T(1)-weighted MRI of a diffusable tracer: standardized quantities and symbols. J Magn Reson Imaging. 1999;10(3):223-232. doi:10.1002/(sici)1522-2586(199909)10:3<223::aid-jmri2>3.0.co;2-s
14. Jain RK. Normalization of tumor vasculature: an emerging concept in antiangiogenic therapy. Science. 2005;307(5706):58-62. doi:10.1126/science.1104819
15. Springer CS Jr, Li X, Tudorica LA, et al. Intratumor mapping of intracellular water lifetime: metabolic images of breast cancer?. NMR Biomed. 2014;27(7):760-773. doi:10.1002/nbm.3111
16. H. Akaike, "A new look at the statistical model identification," in IEEE Transactions on Automatic Control, vol. 19, no. 6, pp. 716-723, December 1974, doi: 10.1109/TAC.1974.1100705.
17. Gillies RJ, Kinahan PE, Hricak H. Radiomics: Images Are More than Pictures, They Are Data. Radiology. 2016;278(2):563-577. doi:10.1148/radiol.2015151169
18. Zou, H. and Hastie, T. (2005), Regularization and variable selection via the elastic net. Journal of the Royal Statistical Society: Series B (Statistical Methodology), 67: 301-320. https://doi.org/10.1111/j.1467-9868.2005.00503.x
19. Obermeyer Z, Emanuel EJ. Predicting the Future - Big Data, Machine Learning, and Clinical Medicine. N Engl J Med. 2016;375(13):1216-1219. doi:10.1056/NEJMp1606181
20. Lambin P, Leijenaar RTH, Deist TM, et al. Radiomics: the bridge between medical imaging and personalized medicine. Nat Rev Clin Oncol. 2017;14(12):749-762. doi:10.1038/nrclinonc.2017.141
21. Sun YZ, Yan LF, Han Y, et al. Differentiation of Pseudoprogression from True Progressionin Glioblastoma Patients after Standard Treatment: A Machine Learning Strategy Combinedwith Radiomics Features from T1-weighted Contrast-enhanced Imaging. *BMC Med Imaging*. 2021;21(1):17. Published 2021 Feb 3. doi:10.1186/s12880-020-00545-5
22. Bani-Sadr A, Eker OF, Berner LP, et al. Conventional MRI radiomics in patients with suspected early- or pseudo-progression. *Neurooncol Adv*. 2019;1(1):vdz019. Published 2019 Sep 1. doi:10.1093/noajnl/vdz019
23. Ari AP, Akkurt BH, Musigmann M, et al. Pseudoprogression prediction in high grade primary CNS tumors by use of radiomics. *Sci Rep*. 2022;12(1):5915. Published 2022 Apr 8. doi:10.1038/s41598-022-09945-9
24. Pak E, Choi KS, Choi SH, et al. Prediction of Prognosis in Glioblastoma Using Radiomics Features of Dynamic Contrast-Enhanced MRI. *Korean J Radiol*. 2021;22(9):1514-1524. doi:10.3348/kjr.2020.1433
25. Bauer AH, Erly W, Moser FG, Maya M, Nael K. Differentiation of solitary brain metastasis from glioblastoma multiforme: a predictive multiparametric approach using combined MR diffusion and perfusion. *Neuroradiology*. 2015;57(7):697-703. doi:10.1007/s00234-015-1524-6
26. O'Neill AF, Qin L, Wen PY, de Groot JF, Van den Abbeele AD, Yap JT. Demonstration of DCE-MRI as an early pharmacodynamic biomarker of response to VEGF Trap in glioblastoma. *J Neurooncol*. 2016;130(3):495-503. doi:10.1007/s11060-016-2243-5
27. Bani Sadr A, Eker OF, Berner L, et al. P13.02 Conventional MRI radiomics in the diagnosis of early- and pseudo-progression. *Neuro Oncol*. 2019;21(Suppl 3):iii62. doi:10.1093/neuonc/noz126.223

References

28. Liu C, Ding J, Spuhler K, et al. Preoperative prediction of sentinel lymph node metastasis in breast cancer by radiomic signatures from dynamic contrast-enhanced MRI. *J Magn Reson Imaging*. 2019;49(1):131-140. doi:10.1002/jmri.26224
29. Wang J, Chen J, Zhou R, Gao Y, Li J. Machine learning-based multiparametric MRI radiomics for predicting poor responders after neoadjuvant chemoradiotherapy in rectal Cancer patients. *BMC Cancer*. 2022;22(1):420. Published 2022 Apr 19. doi:10.1186/s12885-022-09518-z
30. Cheng Y, Xu S, Wang H, et al. Intra- and peri-tumoral radiomics for predicting the sentinel lymph node metastasis in breast cancer based on preoperative mammography and MRI. *Front Oncol*. 2022;12:1047572. Published 2022 Dec 12. doi:10.3389/fonc.2022.1047572
31. Singh G, Manjila S, Sakla N, et al. Radiomics and radiogenomics in gliomas: a contemporary update. *Br J Cancer*. 2021;125(5):641-657. doi:10.1038/s41416-021-01387-w
32. Stupp R, Mason WP, van den Bent MJ, et al. Radiotherapy plus concomitant and adjuvant temozolomide for glioblastoma. *N Engl J Med*. 2005;352(10):987-996. doi:10.1056/NEJMoa043330
33. Wen PY, Macdonald DR, Reardon DA, et al. Updated response assessment criteria for high-grade gliomas: response assessment in neuro-oncology working group. *J Clin Oncol*. 2010;28(11):1963-1972. doi:10.1200/JCO.2009.26.3541
34. Okada H, Weller M, Huang R, et al. Immunotherapy response assessment in neuro-oncology: a report of the RANO working group. *Lancet Oncol*. 2015;16(15):e534-e542. doi:10.1016/S1470-2045(15)00088-1
35. Hegi ME, Diserens AC, Gorlia T, et al. MGMT gene silencing and benefit from temozolomide in glioblastoma. *N Engl J Med*. 2005;352(10):997-1003. doi:10.1056/NEJMoa043331
36. Weller M, van den Bent M, Tonn JC, et al. European Association for Neuro-Oncology (EANO) guideline on the diagnosis and treatment of adult astrocytic and oligodendroglial gliomas. *Lancet Oncol*. 2017;18(6):e315-e329. doi:10.1016/S1470-2045(17)30194-8
37. Parker GJ, Roberts C, Macdonald A, et al. Experimentally-derived functional form for a population-averaged high-temporal-resolution arterial input function for dynamic contrast-enhanced MRI. *Magn Reson Med*. 2006;56(5):993-1000. doi:10.1002/mrm.21066
38. Rohrer M, Bauer H, Mintorovitch J, Requardt M, Weinmann HJ. Comparison of magnetic properties of MRI contrast media solutions at different magnetic field strengths. *Invest Radiol*. 2005;40(11):715-724. doi:10.1097/01.rli.0000184756.66360.d3
39. Pintaske J, Martirosian P, Graf H, et al. Relaxivity of Gadopentetate Dimeglumine (Magnevist), Gadobutrol (Gadovist), and Gadobenate Dimeglumine (MultiHance) in human blood plasma at 0.2, 1.5, and 3 Tesla. *Invest Radiol*. 2006;41(3):213-221. doi:10.1097/01.rli.0000197668.44926.f7
40. Stanisz GJ, Odrobina EE, Pun J, et al. T1, T2 relaxation and magnetization transfer in tissue at 3T. *Magn Reson Med*. 2005;54(3):507-512. doi:10.1002/mrm.20605
41. Shin W, Cashen TA, Horowitz SW, Sawlani R, Carroll TJ. Quantitative CBV measurement from static T1 changes in tissue and correction for intravascular water exchange. *Magn Reson Med*. 2006;56(1):138-145. doi:10.1002/mrm.20937
42. Sourbron SP, Buckley DL. On the scope and interpretation of the Tofts models for DCE-MRI. *Magn Reson Med*. 2011;66(3):735-745. doi:10.1002/mrm.22861
43. Li X, Rooney WD, Springer CS Jr. A unified magnetic resonance imaging pharmacokinetic theory: intravascular and extracellular contrast reagents. *Magn Reson Med*. 2005;54(6):1351-1359. doi:10.1002/mrm.20684
44. Buckley DL, Shurrab AE, Cheung CM, Jones AP, Mamtora H, Kalra PA. Measurement of single kidney function using dynamic contrast-enhanced MRI: comparison of two models in human subjects. *J Magn Reson Imaging*. 2006;24(5):1117-1123. doi:10.1002/jmri.20699
45. Heye AK, Culling RD, Valdés Hernández Mdel C, Thrippleton MJ, Wardlaw JM. Assessment of blood-brain barrier disruption using dynamic contrast-enhanced MRI. A systematic review. *Neuroimage Clin*. 2014;6:262-274. Published 2014 Sep 10. doi:10.1016/j.nicl.2014.09.002
46. Lowekamp BC, Chen DT, Ibáñez L, Blezek D. The Design of SimpleITK. *Front Neuroinform*. 2013;7:45. Published 2013 Dec 30. doi:10.3389/fninf.2013.00045
47. Yaniv Z, Lowekamp BC, Johnson HJ, Beare R. SimpleITK Image-Analysis Notebooks: a Collaborative Environment for Education and Reproducible Research. *J Digit Imaging*. 2018;31(3):290-303. doi:10.1007/s10278-017-0037-8
48. Isensee F, Jaeger PF, Kohl SAA, Petersen J, Maier-Hein KH. nnU-Net: a self-configuring method for deep learning-based biomedical image segmentation. *Nat Methods*. 2021;18(2):203-211. doi:10.1038/s41592-020-01008-z
49. Menze BH, Jakab A, Bauer S, et al. The Multimodal Brain Tumor Image Segmentation Benchmark (BRATS). *IEEE Trans Med Imaging*. 2015;34(10):1993-2024. doi:10.1109/TMI.2014.2377694
50. Bakas S, Akbari H, Sotiras A, et al. Advancing The Cancer Genome Atlas glioma MRI collections with expert segmentation labels and radiomic features. *Sci Data*. 2017;4:170117. Published 2017 Sep 5. doi:10.1038/sdata.2017.117
51. Baid, U., "The RSNA-ASNR-MICCAI BraTS 2021 Benchmark on Brain Tumor Segmentation and Radiogenomic Classification", <i>arXiv e-prints</i>, Art. no. arXiv:2107.02314, 2021. doi:10.48550/arXiv.2107.02314.
52. van Griethuysen JJM, Fedorov A, Parmar C, et al. Computational Radiomics System to Decode the Radiographic Phenotype. *Cancer Res*. 2017;77(21):e104-e107. doi:10.1158/0008-5472.CAN-17-0339
53. Mann, H. B., & Whitney, D. R. (1947). On a Test of Whether one of Two Random Variables is Stochastically Larger than the Other. *Annals of Mathematical Statistics*, *18*(1), 50–60. https://doi.org/10.1214/AOMS/1177730491
54. He, Haibo, Yang Bai, E.A. Garcia, and Shutao Li (2008), "ADASYN: Adaptive synthetic sampling approach for imbalanced learning," *International Joint Conference on Neural Network*, 1322–28.
55. Kingma DP, Ba J. Adam: A method for stochastic optimization. *arXiv*. Published 2014. Accessed April 1, 2026. https://arxiv.org/abs/1106.1813

References

56. Cortes, C., Vapnik, V. Support-vector networks. *Mach Learn* 20, 273–297 (1995). https://doi.org/10.1007/BF00994018
57. Breiman, L. Random Forests. *Machine Learning* 45, 5–32 (2001). https://doi.org/10.1023/A:1010933404324
58. Chen T, Guestrin C. XGBoost: A scalable tree boosting system. arXiv [cs.LG]. 2016:arXiv:1603.02754. Published June 10, 2016. Accessed April 1, 2026. https://arxiv.org/abs/1603.02754
59. Zwanenburg A, Vallières M, Abdalah MA, et al. The Image Biomarker Standardization Initiative: Standardized Quantitative Radiomics for High-Throughput Image-based Phenotyping. *Radiology*. 2020;295(2):328-338. doi:10.1148/radiol.2020191145
60. Shafiq-Ul-Hassan M, Zhang GG, Latifi K, et al. Intrinsic dependencies of CT radiomic features on voxel size and number of gray levels. *Med Phys*. 2017;44(3):1050-1062. doi:10.1002/mp.12123
61. Albert NL, Weller M, Suchorska B, et al. Response Assessment in Neuro-Oncology working group and European Association for Neuro-Oncology recommendations for the clinical use of PET imaging in gliomas. *Neuro Oncol*. 2016;18(9):1199-1208. doi:10.1093/neuonc/now058
62. Bady P, Delorenzi M, Hegi ME. Sensitivity Analysis of the MGMT-STP27 Model and Impact of Genetic and Epigenetic Context to Predict the MGMT Methylation Status in Gliomas and Other Tumors. *J Mol Diagn*. 2016;18(3):350-361. doi:10.1016/j.jmoldx.2015.11.009
63. Ellingson BM, Wen PY, Cloughesy TF. Modified Criteria for Radiographic Response Assessment in Glioblastoma Clinical Trials. *Neurotherapeutics*. 2017;14(2):307-320. doi:10.1007/s13311-016-0507-6
64. Strobl C, Boulesteix AL, Zeileis A, Hothorn T. Bias in random forest variable importance measures: illustrations, sources and a solution. *BMC Bioinformatics*. 2007;8:25. Published 2007 Jan 25. doi:10.1186/1471-2105-8-25

Supplementary

Supplementary

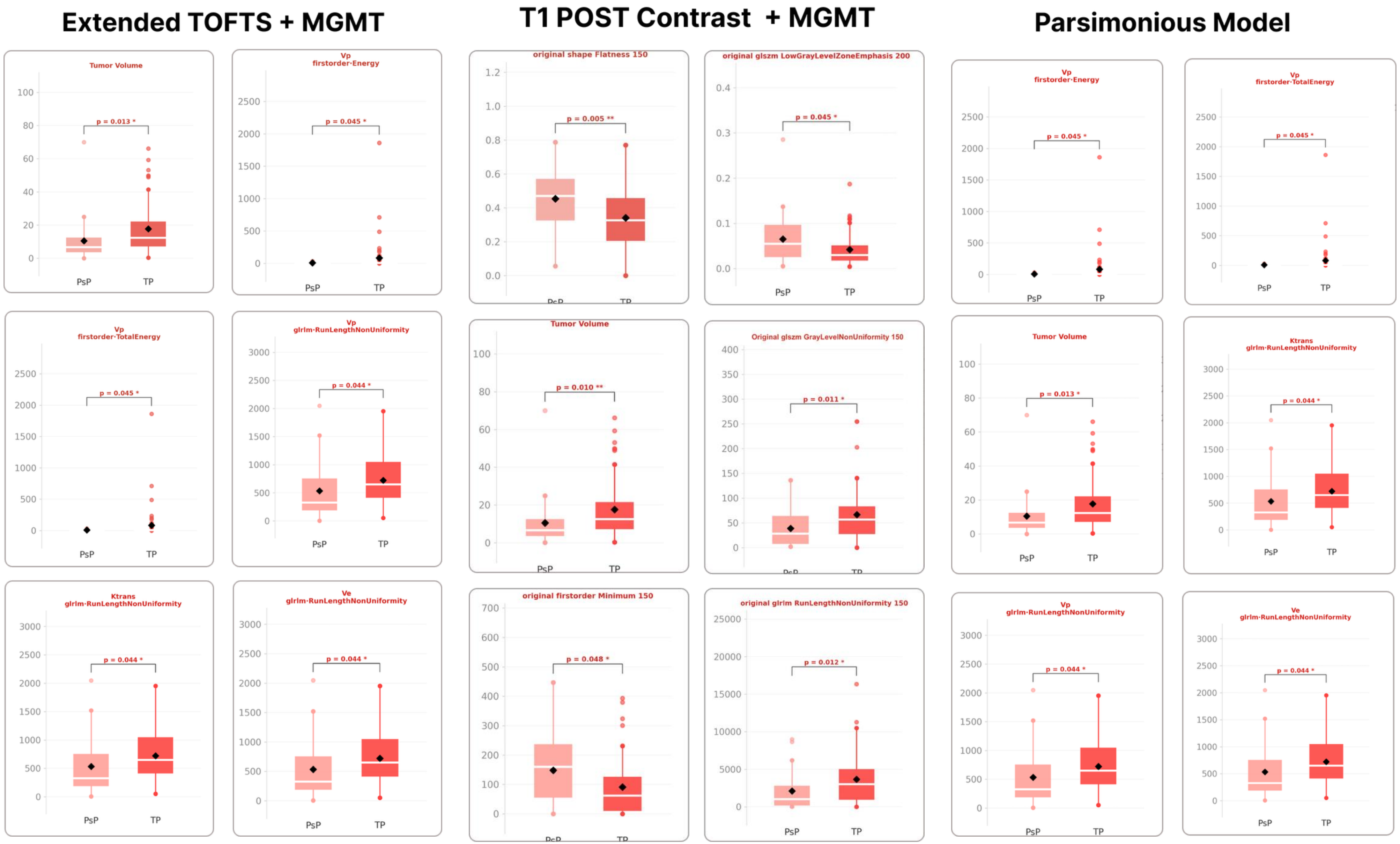

Thank You

Backup Slides

Don’t show them. In case of rendering issue paste these slides.

K^{trans}

Volume Transfer Constant

Rate at which contrast moves from plasma to the Extravascular Extracellular Space (EES)

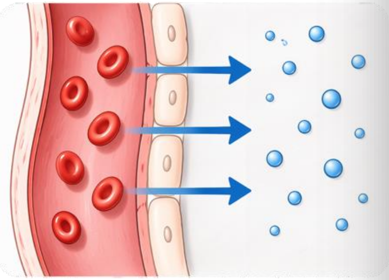

Reflects Capillary Permeability & Surface Area

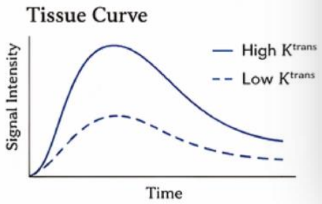

V_e

EES Volume Fraction

Fraction of tissue volume occupied by the Extravascular and Extracellular Space

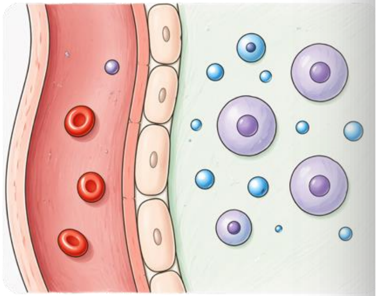

Increased in edema/necrosis
& lower in dense tumour

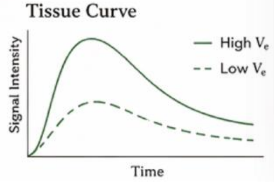

V_p

Plasma Volume Fraction

Fraction of tissue volume occupied by plasma (intravascular space).A

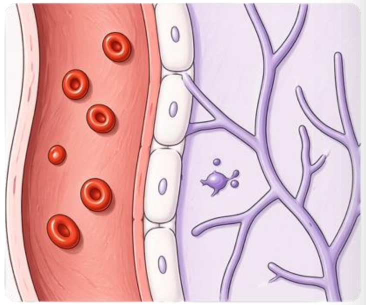

Reflects vascular Volume or Density

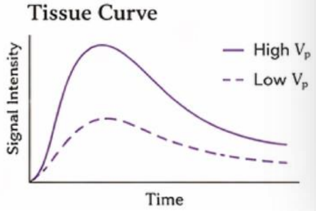

F_p

Plasma Flow Rate

Rate of plasma flowing throug the capillary bed per unit tissu volume.

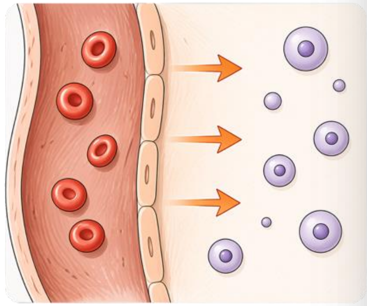

resents tissue Perfusion

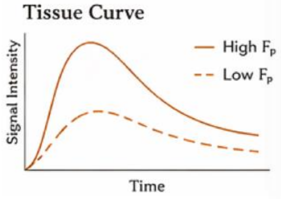

τ_i

Intracellular Water Lifetime

Average time water molecules spend inside cells.

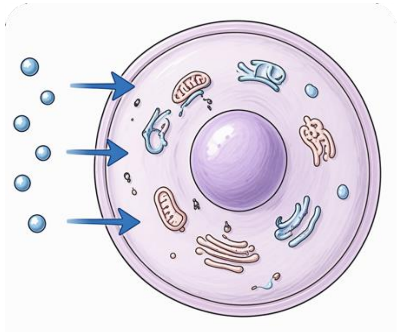

Shorter τ implies higher cell membrane

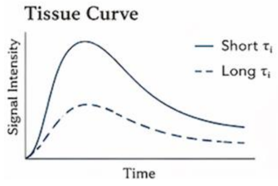

+

Foundations

A medical scan shows structure, not always clear meaning.

Medical images, specially Magnetic Resonance Imaging give us a detailed view of what's inside the body. We can see shapes, boundaries, and visible biological changes. But not every important detail is clearly obvious. Some differences are very subtle and obvious to overlook, especially in the early stages. So even though the information is there, understanding it completely is not always convenient !

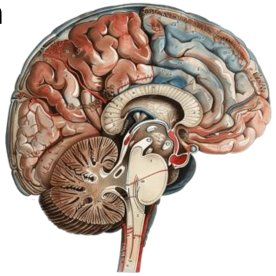

Foundations

TP and PSP Often Indistinguishable on Conventional MRI

Both show contrast enhancement and lesion growth due to blood–brain barrier disruption, making them difficult to distinguish.

DICOM Credit : University of Toronto (University Health Network, UHN)

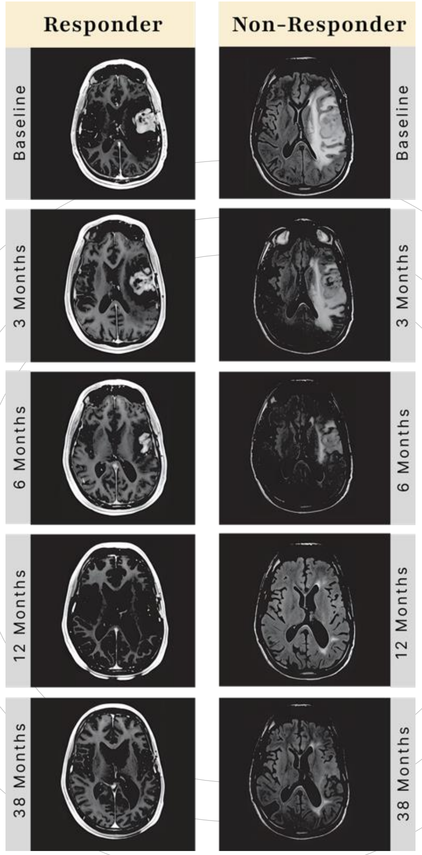

Foundations

Clinical Consequences of Misclassification

Clinically, this is important. In glioblastoma, different tumour regions can show similar post-treatment changes, making TP and PsP look alike. This can lead to misclassification, resulting in either unnecessary treatment changes or delayed intervention.

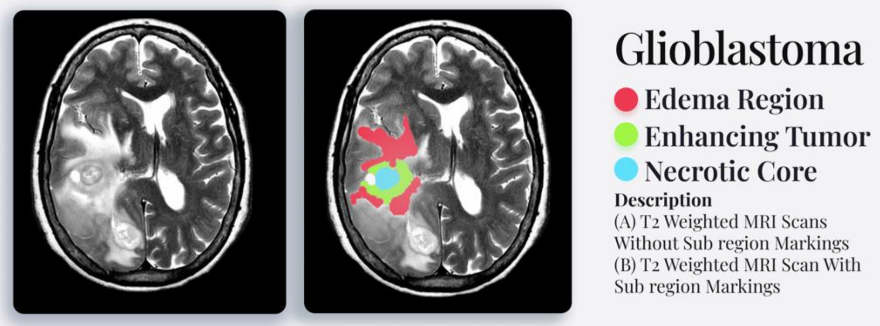

Image Credit : University of Pennsylvania Multi modal Brain Tumor Segmentation Challenge 2020

Foundations

A medical scan shows structure, not always clear meaning.

Despite advances, widely used software from vendors like GE, Siemens, Philips, along with **conventional models**, remain limited in reliably distinguishing TP from PsP due to imaging overlap. Most approaches report performance ≤75% in accuracy. In this work, we adopt a fundamentally novel approach, achieving improved performance with an AUC of 0.89 and an F1-score of 0.90 [Different Gradient Coils too]

Foundations

TP vs PSP for Several Parametric Maps

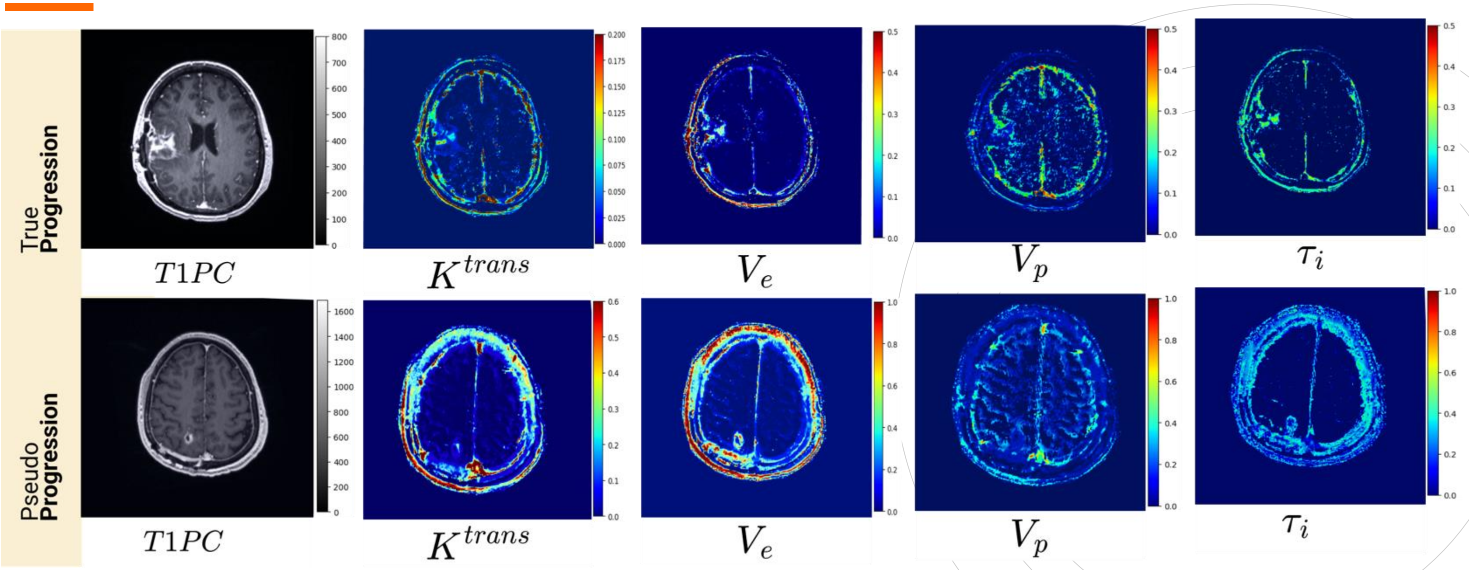

DICOM Credit : University of Pennsylvania

When Imaging isn't
ENOUGH

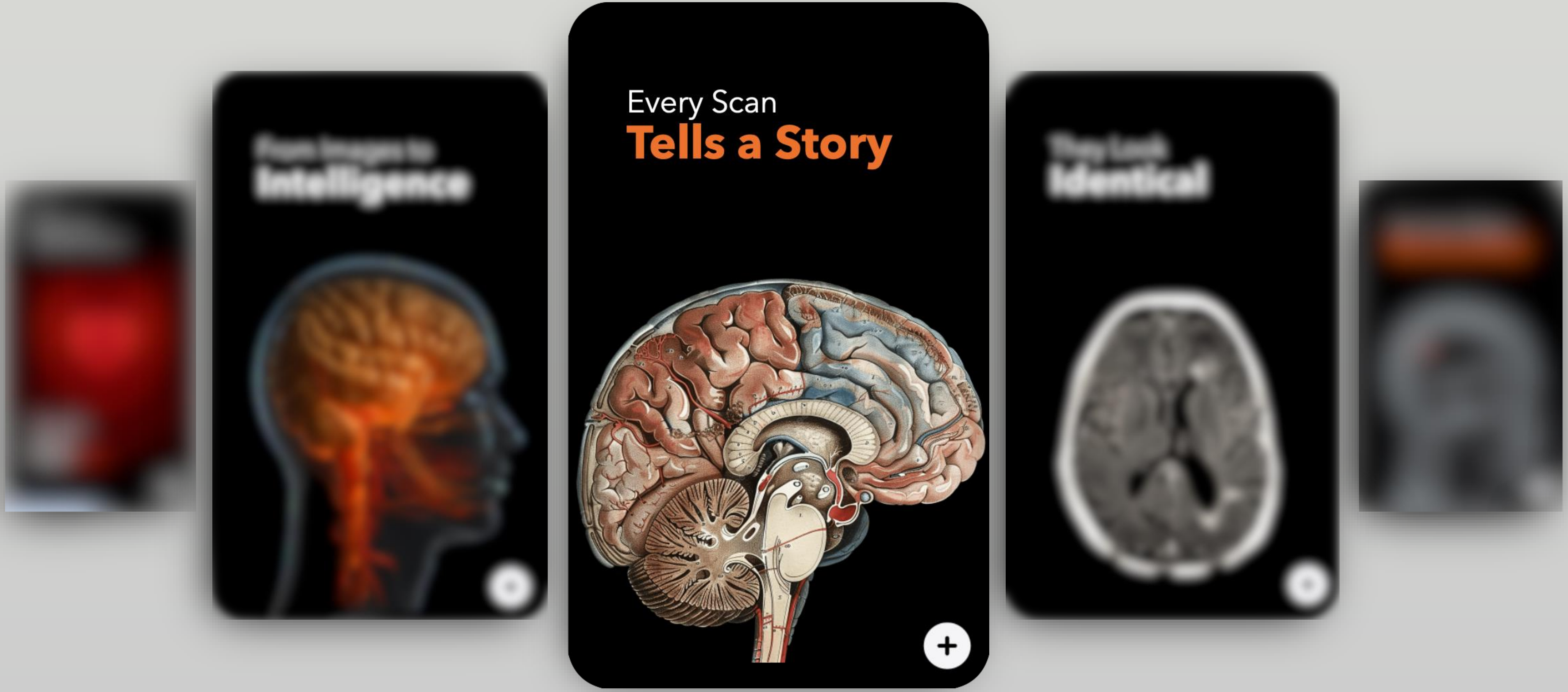

When Imaging isn't
ENOUGH

Every Scan
Tells a Story

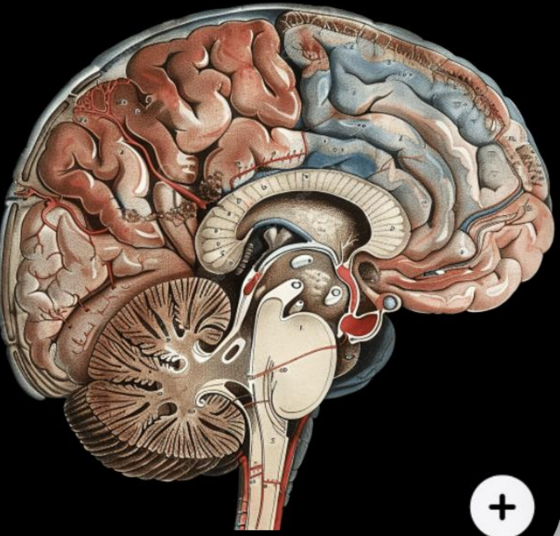

They Look
Identical

The Cost of Being
Misclassified

From Images to
Intelligence

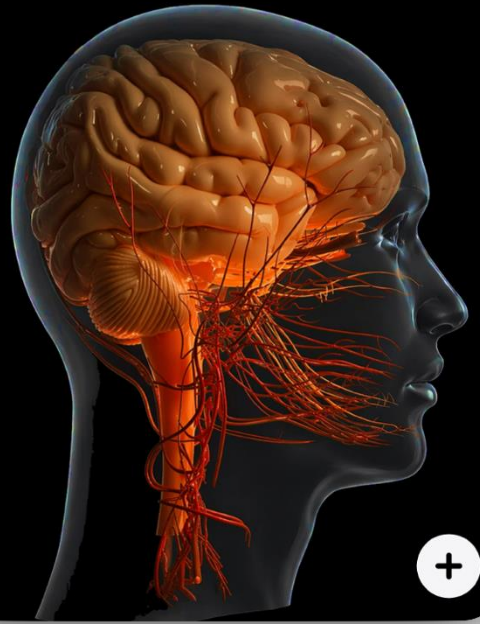

When Imaging isn't
ENOUGH

Every Scan
Tells a Story

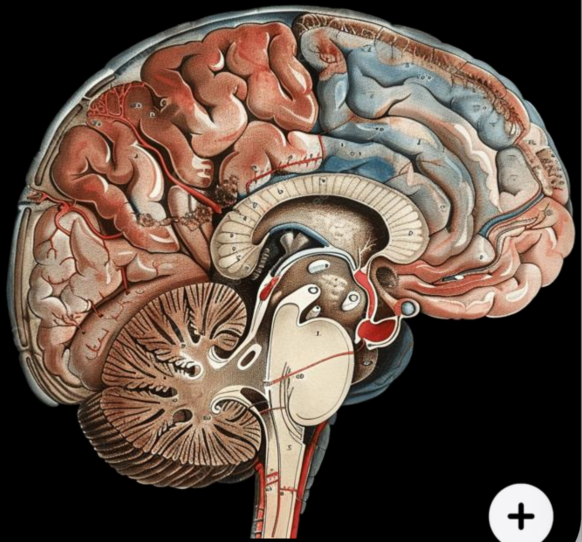

They Look
Identical

The Cost of Being
Misclassified

From Images to
Intelligence